

Deterministic approach to microscopic three-phase traffic theory

Boris S. Kerner ¹ and Sergey L. Klenov ²

¹ DaimlerChrysler AG, REI/VF, HPC: G021, 71059 Sindelfingen, Germany

² Moscow Institute of Physics and Technology, Department of Physics, 141700 Dolgoprudny, Moscow Region, Russia

PACS numbers: 89.40.+k, 47.54.+r, 64.60.Cn, 64.60.Lx

Abstract. A deterministic approach to three-phase traffic theory is presented. Two different deterministic microscopic traffic flow models are introduced. In an acceleration time delay model (ATD-model), different time delays in driver acceleration associated with driver behavior in various local driving situations are explicitly incorporated into the model. Vehicle acceleration depends on local traffic situation, i.e., whether a driver is within the free flow, or synchronized flow, or else wide moving jam traffic phase. In a speed adaptation model (SA-model), driver time delays are simulated as a model effect: Rather than driver acceleration, vehicle speed adaptation occurs with different time delays depending on one of the three traffic phases in which the vehicle is in. It is found that the ATD- and SA-models show spatiotemporal congested traffic patterns that are adequate with empirical results. It is shown that in accordance with empirical results in the ATD- and SA-models the onset of congestion in free flow at a freeway bottleneck is associated with a first-order phase transition from free flow to synchronized flow. As in empirical observations, in the ATD- and SA-models moving jams emerge spontaneously in synchronized flow only. Differences between the ATD- and SA-models are studied. A comparison of the ATD- and SA-models with stochastic models in the context of three phase traffic theory is made. A critical discussion of earlier traffic flow theories and models based on the fundamental diagram approach is presented.

1. Introduction

Theoretical studies of freeway traffic flow dynamics is one of the rapid developing fields of statistical and nonlinear physics. For a mathematical description of freeway traffic flow different deterministic and stochastic traffic flow models have been introduced (see the reviews [1, 2, 3, 4, 5, 6], the book [7], and the conference proceedings [8, 9, 10, 11, 12, 13, 14, 15]). In deterministic models, some dynamic rules of vehicle motion in traffic flow are responsible for spatiotemporal features of traffic patterns that the models exhibit. Contrastingly, stochastic models, in addition to dynamic rules of vehicle motion, exhibit model fluctuations, which play a fundamental role for traffic pattern features.

There are at least two classes of deterministic traffic flow models [1, 3, 4, 5, 6]. In the first class, driver time delays in vehicle acceleration (deceleration) a associated with a change in local driving situation are explicitly taken into account. An example is the classic model of Herman, Montroll, Potts, and Rothery [16]: If the vehicle speed v , or the speed difference between the vehicle speed and the speed of the preceding vehicle v_ℓ , or else the net distance g (space gap) between vehicles changes, then the driver accelerates (decelerates) with a time delay τ [16]:

$$a(t + \tau) = f(v(t), v_\ell(t), g(t)). \quad (1)$$

After integration of Eq. (1) and choosing of the integrating constant associated with steady state model solutions that lie on a one-dimensional curve in the flow–density plane (the fundamental diagram), a solvable traffic flow model is gained as that of Gazis, Herman, and Rothery [17]; this model is similar to the classic model of Newell [20] (see the review by Nagel et al. [6] for more detail). Recall that steady state solutions are hypothetical model solutions in which all vehicles move at the same time-independent speed and the same space gap between vehicles. One of the mathematical descriptions of this model class first proposed by Nagatani and Nakanishi [18] and further developed by Lubashevky et al. [19] reads as follows

$$\frac{da}{dt} = \frac{f(v(t), v_\ell(t), g(t)) - a(t)}{\tau}. \quad (2)$$

In both models [17, 18, 19], steady state model solutions in the flow–density plane lie on the fundamental diagram.

There is also another class of deterministic microscopic models in which the vehicle speed satisfies the equation [1, 3, 4, 5, 6]:

$$\frac{dv}{dt} = \phi(v, v_\ell, g). \quad (3)$$

Examples are optimal velocity (OV) models of Newell [20], Whitham [21], Bando, Sugiyama et al. [22], and the intelligent driver model (IDM) of Treiber and Helbing [23, 24]. Steady state solutions of this model class that obviously satisfy the conditions $\phi(v, v_\ell, g) = 0$ and $v = v_\ell$ lie on the fundamental diagram in the flow–density plane.

If functions and model parameters in the models (2) and (3) are chosen in an appropriated way, then there is a range of vehicle density in which steady state model solutions are unstable against infinitesimal inhomogeneous perturbations in free flow [2, 3, 4, 5, 6]. Whereas in the models of the first class this instability is the result of driver delay time τ (2), in the second class models (3) the instability is a model effect. This effect is simulated by a density dependent dynamic behavior of inhomogeneous model solutions in the vicinity of model steady states on the fundamental diagram.

The growth of local perturbations caused by this instability leads to spontaneous moving jam emergence in free flow. The models whose steady states lie on the fundamental diagram and in which moving jams emerge spontaneously in free flow, specifically, the onset of congestion in free flow is caused by moving jam emergence [3, 4, 5, 6] are associated with the fundamental diagram approach to traffic flow theories [7]. Consequently, in these models at an on-ramp bottleneck moving jam(s) occurs spontaneously in free flow when the flow rate upstream of the bottleneck q_{in} is high enough and the flow rate to the on-ramp q_{on} increases gradually beginning from zero [4, 5, 25, 26, 27, 24].

However, this fundamental model result (i.e., that at a high enough flow rate on the main road the phase transition governing the onset of congestion in free flow is associated with spontaneous moving jam emergence [3, 4, 5, 6]) is in a serious conflict with empirical evidence [28, 29, 7].

Indeed, numerous empirical investigations of phase transitions in freeway traffic indicate that moving jams do *not* emerge spontaneously in free flow. Rather than moving jam emergence, a first-order phase transition from free flow to synchronized flow (F→S transition for short) governs the onset of congestion in free flow [28, 29]. Due to the F→S transition, the speed decreases abruptly. This speed breakdown caused by the F→S transition that is also called traffic breakdown exhibits a probabilistic nature [30, 31, 32]: At the same traffic demand (the same flow rates q_{in} and q_{on}), in some realizations (days) traffic breakdown, i.e., an F→S transition is observed, but in other realizations it is not observed. The probabilistic nature of traffic breakdown is explained by the metastability and nucleation effects, which are characteristic features of the first-order F→S transition [7].

There are the macroscopic spatiotemporal *objective* (empirical) criteria for the two different phases in congested traffic, synchronized flow and wide moving jam [7]: A wide moving jam propagates through any flow states and bottlenecks while maintaining the mean velocity of the downstream jam front. In contrast, the downstream front of synchronized flow, in which vehicles accelerate from synchronized flow upstream to free flow downstream, is usually fixed at a freeway bottleneck.

Wide moving jams can emerge spontaneously only in the synchronized flow phase (S→J transition for short). Thus, in empirical observations wide moving jams occur spontaneously due to the sequence of two phase transitions, first an F→S transition, then later and usually at another location an S→J transition (F→S→J transitions for short) [7].

Consequently, in 1996–1999 Kerner introduced three-phase traffic theory (see [7] for a review). In this theory, there are three traffic phases: free flow, synchronized flow, and wide moving jams. This theory can explain and predict the F→S→J transitions and empirical spatiotemporal congested pattern features. The fundamental hypothesis of three-phase traffic theory, which is a qualitative theory, is that hypothetical steady states of synchronized flow cover a two-dimension region in the flow–density plane, i.e., there is no fundamental diagram in this theory.

The first microscopic models in the context of three-phase traffic theory introduced in 2002 are stochastic models [33, 34]. These models exhibit the F→S→J transitions as well as all types of congested patterns found in empirical observations [33, 34, 35, 36, 7, 37]. Recently, some new microscopic models based on three-phase traffic theory have been developed [38, 39, 40]. However, there are no deterministic models in the context of three-phase traffic theory, which can exhibit the F→S→J transitions and the diagram of congested patterns of three-phase traffic

theory [29, 7]. In stochastic models [33, 34, 35, 36, 7], driver time delays in acceleration (deceleration) are simulated mainly through the use of model fluctuations. Therefore, a development of deterministic models based on three-phase theory is important for a more realistic theory of car following behavior.

In this paper, two deterministic microscopic three-phase traffic models are presented. In an acceleration time delay model (Sect. 2), an explicit description of driver time delays in vehicle acceleration (deceleration) is used. In a speed adaptation model (Sect. 3), a speed and density dependent dynamic behavior of model solutions in the vicinity of *averaged* steady states of synchronized flow associated with a one-dimension region in the flow–density plane is applied, to simulate phase transitions and congested patterns. In Sect. 4, we show that these models exhibit the F→S→J transitions and congested patterns associated with results of empirical observations. In addition, a stochastic speed adaptation model is introduced and compared with the deterministic speed adaptation model of Sect. 3. In Sect. 5, the deterministic microscopic three-phase traffic models of Sects. 2 and 3 are compared with earlier deterministic models and a critical discussion of models in the context of the fundamental diagram approach is performed.

2. Acceleration Time Delay Model

2.1. Main Equations

A deterministic three-phase traffic flow model with driver time delays (**A**cceleration **T**ime **D**elay model, ATD-model for short) reads as follows:

$$\frac{dx}{dt} = v, \quad (4)$$

$$\frac{dv}{dt} = a, \quad (5)$$

$$\frac{da}{dt} = \begin{cases} (a^{(\text{free})} - a)/\tau & \text{at } g > G \text{ and } g > g_{\text{max}}^{(\text{jam})}, \\ (a^{(\text{syn})} - a)/\tau & \text{at } g \leq G \text{ and } g > g_{\text{max}}^{(\text{jam})}, \\ (a^{(\text{jam})} - a)/\tau & \text{at } 0 \leq g \leq g_{\text{max}}^{(\text{jam})}, \end{cases} \quad (6)$$

where x , v , and a are the space co-ordinate, the speed, and the acceleration of a vehicle, respectively; $g = x_\ell - x - d$ is the space gap (net distance) to the preceding vehicle; the lower index ℓ marks variables related to the preceding vehicle; all vehicles have the same length d , which includes the minimum space gap between vehicles within a wide moving jam; $G = G(v, v_\ell)$ is a synchronization gap (see Sect. 2.5); $a^{(\text{free})}$, $a^{(\text{syn})}$, and $a^{(\text{jam})}$ are vehicle accelerations in the free flow, synchronized flow, and wide moving jam phases, respectively. If the space gap g satisfies the condition $g > G(v, v_\ell)$, then a vehicle moves in accordance with the rules for free flow. Within synchronized flow associated with the condition $g_{\text{jam}}^{(\text{max})} < g \leq G(v, v_\ell)$, the vehicle tends to adapt the speed to the preceding vehicle. Within a wide moving jam, the space gap is small, specifically $g \leq g_{\text{jam}}^{(\text{max})}$, and the vehicle decelerates; $g_{\text{max}}^{(\text{jam})}$ is the maximum space gap within the wide moving jam phase. In (6), τ is a driver time delay.

2.2. Driver Acceleration

The accelerations (decelerations) $a^{(\text{free})}$, $a^{(\text{syn})}$, and $a^{(\text{jam})}$ are found from the condition

$$a^{(\text{phase})} = \min(\max(\tilde{a}^{(\text{phase})}, a_{\text{min}}), a_{\text{max}}, a_s), \quad (7)$$

the superscript “phase” in (7) means either “free”, or “syn”, or else “jam” for the related traffic phase; a_s is an acceleration related to safety requirements; a_{\min} and a_{\max} ($a_{\min} < 0$, $a_{\max} \geq 0$) are respectively the minimum and maximum accelerations for cases in which there are no safety restrictions. ‡ In (7), functions $\tilde{a}^{(\text{free})}$, $\tilde{a}^{(\text{syn})}$, and $\tilde{a}^{(\text{jam})}$ associated with driver acceleration within the related traffic phase – free flow, or synchronized flow, or else wide moving jam – are determined as follows:

$$\begin{aligned} \tilde{a}^{(\text{free})}(g, v, v_\ell) &= A^{(\text{free})}(g, v)(V^{(\text{free})}(g) - v) + \\ &K^{(\text{free})}(v, v_\ell)(v_\ell - v), \end{aligned} \quad (9)$$

$$\begin{aligned} \tilde{a}^{(\text{syn})}(g, v, v_\ell) &= A^{(\text{syn})} \min(V_{\max}^{(\text{syn})}(g) - v, 0) + \\ &K^{(\text{syn})}(v, v_\ell)(v_\ell - v), \end{aligned} \quad (10)$$

$$\tilde{a}^{(\text{jam})}(v) = -K^{(\text{jam})}(v)v. \quad (11)$$

Here $V^{(\text{free})}(g)$ is a gap-dependent optimal speed in free flow; $V_{\max}^{(\text{syn})}(g)$ is a gap-dependent maximum vehicle speed in steady states of synchronized flow; $A^{(\text{free})}$, $A^{(\text{syn})}$, $K^{(\text{free})}$, $K^{(\text{syn})}$, and $K^{(\text{jam})}$ are sensitivities. In real traffic, these sensitivities can be asymmetric speed functions depending on whether the vehicle speed is higher or lower than either the speed of the preceding vehicle or the optimal speed $V^{(\text{free})}(g)$ (see Sect. 2.5).

The acceleration a_s for safety vehicle motion is chosen as (Appendix A)

$$a_s(g, v, v_\ell) = \alpha \frac{g - vT_s + (T_0 + v_\ell/b)(v_\ell - v)}{T_0(T_s + v_\ell/b)}, \quad (12)$$

where T_s is a safety time gap; b , T_0 and α are constants. § Formula (12) ensures collision less vehicle motion at all chosen model parameters.

2.3. Physics of Driver Time Delays

In Eqs. (6), the time delay τ is chosen as

$$\tau = \begin{cases} \tau_s & \text{at } a_s < \min(0, \tilde{a}^{(\text{phase})}, a), \\ \tilde{\tau} & \text{otherwise.} \end{cases} \quad (15)$$

Here, τ_s is a short driver time delay associated with a finite driver reaction time that must be taken into account in the cases when the driver should decelerate unexpectedly

‡ Since the vehicle speed v cannot be negative, the following condition is also used for Eqs. (5), (6):

$$a(t) \geq 0 \text{ at } v(t) = 0. \quad (8)$$

To satisfy this condition in numerical simulation, the acceleration $a(t)$ is replaced by the value $\max(a(t), 0)$ if $v(t) = 0$ at time t .

§ Note that Eqs. (6) of the ATD-model can also be written without the term $a^{(\text{jam})}$ as follows

$$\frac{da}{dt} = \begin{cases} (a^{(\text{free})} - a)/\tau & \text{at } g > G, \\ (a^{(\text{syn})} - a)/\tau & \text{at } g \leq G, \end{cases} \quad (13)$$

if rather than (12) the following formula is used for the safety acceleration in (7)

$$a_s = \alpha \begin{cases} \frac{g - vT_s + (T_0 + v_\ell/b)(v_\ell - v)}{T_0(T_s + v_\ell/b)}, & \text{at } g \geq g_{\max}^{(\text{jam})}, \\ \frac{-v(T_s + T_0)}{T_0 T_s}, & \text{at } g < g_{\max}^{(\text{jam})}. \end{cases} \quad (14)$$

In this case, the second term in the right hand side of Eq. (14) plays the role of vehicle acceleration within the wide moving jam phase.

to avoid collisions; $\tilde{\tau}$ is a time delay in other traffic situations, which is chosen different depending on whether the vehicle accelerates or decelerates:

$$\tilde{\tau} = \begin{cases} \tau^{(\text{acc})} & \text{at } a > 0, \\ \tau^{(\text{dec})} & \text{at } a \leq 0. \end{cases} \quad (16)$$

In turn, $\tau^{(\text{acc})}$ and $\tau^{(\text{dec})}$ in (16) depend on the acceleration a :

$$\tau^{(\text{acc})} = \begin{cases} \tau_0^{(\text{acc})} & \text{at } a < \tilde{a}^{(\text{phase})}, \\ \tau_1^{(\text{acc})} & \text{otherwise,} \end{cases} \quad (17)$$

$$\tau^{(\text{dec})} = \begin{cases} \tau_0^{(\text{dec})} & \text{at } a \geq \tilde{a}^{(\text{phase})}, \\ \tau_1^{(\text{dec})} & \text{otherwise.} \end{cases} \quad (18)$$

The driver time delays $\tau_0^{(\text{acc})}$, $\tau_0^{(\text{dec})}$, $\tau_1^{(\text{dec})}$, and $\tau_1^{(\text{acc})}$ in (17), (18) are associated with human expectation of local driving conditions, in particular, with spatial and temporal anticipation of a driver in accordance with local adaptation to those traffic situations in which the driver takes into account the behavior of many vehicles ahead.

$\tau_0^{(\text{acc})}$ is the mean time delay when a driver starts to accelerate or wants to increase the acceleration. This can often occur at the downstream front of a wide moving jam or a synchronized flow region, i.e., when the speed in traffic flow downstream of the vehicle is higher than the current vehicle speed. In these cases, after the preceding vehicle has begun to accelerate, the driver also begins to accelerate, however, after a time delay to have a desired time gap to the preceding vehicle.

$\tau_0^{(\text{dec})}$ is the mean time delay when the driver starts to decelerate or wants to decelerate harder in cases in which the driver approaches a region of a lower speed downstream.

$\tau_1^{(\text{acc})}$ corresponds to situations in which the driver accelerates currently but wants either to stop the acceleration or to reduce it. Thus, $\tau_1^{(\text{acc})}$ is the mean driver time delay in interruption or reduction of driver acceleration in cases in which the driver recognizes that current acceleration is greater than a desired acceleration in the current driving situation.

$\tau_1^{(\text{dec})}$ corresponds to situations in which the driver decelerates currently but wants either to stop the deceleration or to reduce it. Thus, $\tau_1^{(\text{dec})}$ is the mean time delay in interruption or reduction of driver deceleration in cases in which the driver recognizes that current deceleration is more negative than a desired deceleration in the current driving situation.

2.4. Model of Road with On-Ramp Bottleneck

“Open” boundary conditions are applied. At the beginning of the road free flow conditions are generated for each vehicle one after another at equal time intervals $\tau_{\text{in}} = 1/q_{\text{in}}$ where q_{in} is the flow rate in the incoming boundary flow. However, a new vehicle appears only if the distance from the beginning of the road ($x = x_{\text{b}}$) to the position $x = x_{\ell}$ of the farthest upstream vehicle in the lane exceeds the distance $v_{\ell}T_{\text{s}} + d$ where $T_{\text{s}} = 1 \text{ s}$ is a safety time gap. The speed v and coordinate x of a new vehicle are $v = v_{\ell}$ and $x = x_{\text{b}}$, respectively.

In the initial state ($t = 0$), all vehicles have the same initial speed $v = v_{\text{h}} = V^{(\text{free})}(g_{\text{h}})$, where g_{h} is an initial space gap between vehicles and $q_{\text{in}} = v_{\text{h}}/(g_{\text{h}} + d)$.

After a vehicle has reached the end of the road, it is removed; before this, the farthest downstream vehicle maintains its speed.

An on-ramp bottleneck on the main road is considered. The on-ramp consists of two parts: (i) The merging region of the length L_m at which vehicle can merge onto the main road from the on-ramp. (ii) The part of the on-ramp lane of length L_r upstream of the merging region at which vehicles move according to the model equations for a homogeneous road with the maximum speed $v_{\text{free, on}} = 60$ km/h. At the beginning of the on-ramp lane $x = x_{\text{on}}^{(b)}$ the flow rate to the on-ramp q_{on} is given as the flow rate on the main road q_{in} .

The following rules are applied for vehicle merging within the merging region: Firstly, a speed \hat{v} is calculated corresponding to formula

$$\hat{v} = \min(v^+, v + \Delta v_r^{(1)}). \quad (19)$$

Then the speed \hat{v} is used in the merging rules:

$$g^+ > g_{\text{max}}^{(\text{jam})} + \gamma \hat{v} T_s, \quad g^- > g_{\text{max}}^{(\text{jam})} + \gamma v^- T_s. \quad (20)$$

Here superscripts g^+ and g^- are space gaps to the preceding vehicle and the trailing vehicle on the main road, respectively; v^+ and v^- are respectively speeds of the preceding vehicle and the trailing vehicle; γ and $\Delta v_r^{(1)}$ are constants, where $\Delta v_r^{(1)}$ describes the maximum possible increase in speed after merging. Note that the finite increase $\Delta v_r^{(1)}$ in the vehicle speed (19) is used to simulate a complex driver behavior during merging onto the main road, especially in synchronized flow: In some cases, before merging the driver has to accelerate abruptly, to adjust the speed to the speed of the preceding vehicle.

If the conditions (20) are satisfied, then the vehicle merges onto the main road. After merging the vehicle speed v is set to \hat{v} (19) and the vehicle coordinate does not change. If the conditions (20) are not satisfied, the vehicle does not merge onto the main road. In this case, the vehicle moves in the on-ramp lane until it comes to a stop at the end of the merging region.

2.5. Model Functions and Parameters

Model functions and parameters are shown in Tables 1 and 2, respectively.

2.6. Steady States

In steady states, all vehicles have the same speed $v = v_\ell$ and the same space gap g , and all accelerations and their time derivatives are zero, and the density ρ and the flow rate q are related to the space gap g and to the speed v by the obvious conditions

$$\rho = 1/(x_\ell - x) = 1/(g + d), \quad q = \rho v = v/(g + d). \quad (21)$$

According to (5)–(12), for steady states we get

$$v = V(g) \quad \text{at } g > G(v) \text{ and } g > g_{\text{max}}^{(\text{jam})}, \quad (22)$$

$$v \leq V(g) \quad \text{at } g \leq G(v) \text{ and } g > g_{\text{max}}^{(\text{jam})}, \quad (23)$$

$$v = 0 \quad \text{at } g \leq g_{\text{max}}^{(\text{jam})}, \quad (24)$$

where in all three cases

$$g \geq v T_s. \quad (25)$$

Table 1. ATD-model functions

| Synchronization gap |
|---|
| $G(v, v_\ell) = v \max(0, T^{(\text{syn})}(v) + \kappa(v, v_\ell)(v_\ell - v)),$ $\kappa(v, v_\ell) = \begin{cases} \kappa^{(\text{acc})} & \text{at } v < v_\ell, \\ \kappa^{(\text{dec})} & \text{at } v \geq v_\ell, \end{cases}$ $T^{(\text{syn})}(v) = T_0^{(\text{syn})}(1 - 0.85(v/V_0)^2).$ |
| Sensitivities |
| $A^{(\text{free})}(g, v) = A^{(\text{syn})}(g, v) = A_0,$ $K^{(\text{free})}(v, v_\ell) = K^{(\text{syn})}(v, v_\ell) = K(v, v_\ell),$ $K(v, v_\ell) = \begin{cases} K^{(\text{acc})} & \text{at } v < v_\ell, \\ K^{(\text{dec})} & \text{at } v \geq v_\ell. \end{cases}$ $K^{(\text{dec})}(v) = K_1^{(\text{dec})}(1 - \lambda(v)) + K_2^{(\text{dec})}\lambda(v),$ $\lambda(v) = (1 + \exp((v/v_c - 1)/\delta))^{-1}.$ |
| Characteristic speed functions |
| $V^{(\text{free})}(g) = V(g) \quad \text{at } g > g_{\min}^{(\text{free})},$ $V_{\max}^{(\text{syn})}(g) = V(g) \quad \text{at } g \leq g_{\min}^{(\text{free})},$ $V(g) = V_0 \tanh((g + 2)/(V_0 T)),$ <p>$g_{\min}^{(\text{free})}$ is the minimum space gap in free flow found as a solution of the set of the equations $v = V(g)$ and $g = G(v, v_\ell)$ at $v = v_\ell$.</p> |
| Speed dependencies of time delays |
| $\tau_1^{(\text{dec})}(v) = \begin{cases} 0.5 \text{ s} & \text{at } v \geq v_c, \\ 0.7 \text{ s} & \text{otherwise,} \end{cases}$ $\tau_1^{(\text{acc})}(v) = \begin{cases} 0.57 \text{ s} & \text{at } v \geq v_c, \\ 0.87 \text{ s} & \text{otherwise.} \end{cases}$ |

Table 2. ATD-model parameters

| |
|---|
| $V_0 = 33.3 \text{ m/s (120 km/h)}, T = 0.9 \text{ s},$ $A_0 = 0.5 \text{ s}^{-1}, K^{(\text{acc})} = 0.8 \text{ s}^{-1}, K^{(\text{jam})} = 1 \text{ s}^{-1},$ $K_1^{(\text{dec})} = 0.95 \text{ s}^{-1}, K_2^{(\text{dec})} = 0.48 \text{ s}^{-1}, v_c = 15 \text{ m/s}, \delta = 0.15,$ $T_0^{(\text{syn})} = 2.5 \text{ s}, \kappa^{(\text{acc})} = 0.5 \text{ s}^2/\text{m}, \kappa^{(\text{dec})} = 0.55 \text{ s}^2/\text{m},$ $g_{\max}^{(\text{jam})} = 0.95 \text{ m}, \tau_0^{(\text{dec})} = 1 \text{ s}, \tau_0^{(\text{acc})} = 0.75 \text{ s}, \tau_s = 0.4 \text{ s},$ $a_{\max} = 1 \text{ m/s}^2, a_{\min} = -1 \text{ m/s}^2,$ $\alpha = 0.5, b = 4 \text{ m/s}^2, T_s = 1 \text{ s}, T_0 = 0.4 \text{ s},$ $L_m = 300 \text{ m}, L_r = 500 \text{ m}, \gamma = 0.22, \Delta v_r^{(1)} = 8 \text{ m/s}.$ |
|---|

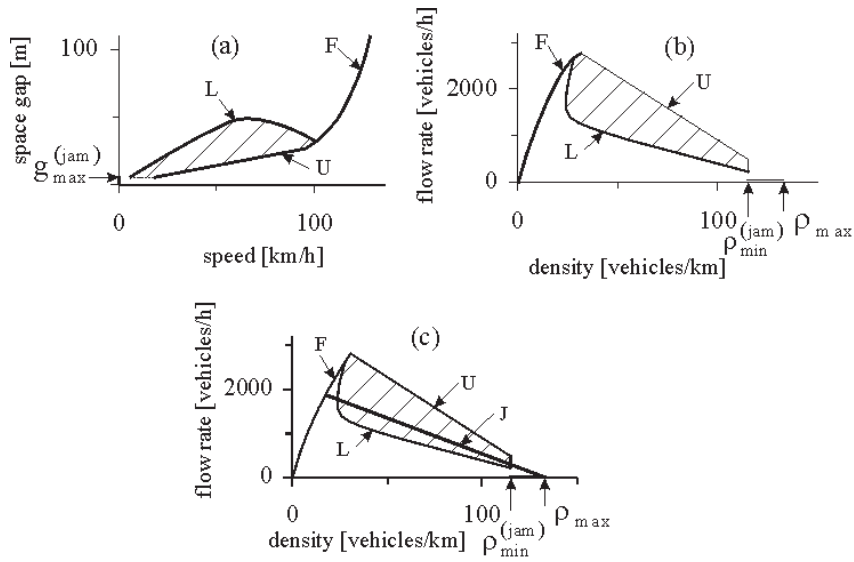


Figure 1. Model steady states for the ADT-model: (a) - in the space-gap-speed plane. (b) - in the flow-density plane. (c) - Steady states and the line *J*.

According to (22)–(25), the model steady states consist of the curve $v = V(g)$ (22) at $g > g_{\min}^{(\text{free})}$ (curve F in Fig. 1 (a)) associated with the free flow phase, a two-dimensional region in the space-gap–speed plane determined by inequalities in (23), (25) associated with the synchronized flow phase, and the line $v = 0$ at $g \leq g_{\max}^{(\text{jam})}$ (24) associated with the wide moving jam phase (Fig. 1 (a)). The two-dimensional region for steady states of synchronized flow is limited by the following boundaries: the line U , the curve L , the curve $v = V(g)$ (22) at $g \leq g_{\min}^{(\text{free})}$, and the horizontal line $g = g_{\max}^{(\text{jam})}$. The boundary U associated with the safe speed is determined by the condition (25) when it is the equality: $g = vT_s$. The boundary L is found from the condition $g = G(v)$.

In the flow–density plane, free flow (curve F in Fig. 1, (b)) is found from

$$q = \rho V_F(\rho) \quad (26)$$

at $\rho < \rho_{\max}^{(\text{free})}$ where $V_F(\rho) = V(g) |_{g=\rho^{-1}-d}$, $\rho_{\max}^{(\text{free})} = (g_{\min}^{(\text{free})} + d)^{-1}$. A wide moving jam is associated with the horizontal line $q = 0$ at $\rho_{\min}^{(\text{jam})} \leq \rho \leq \rho_{\max}$ (Fig. 1 (b)), where $\rho_{\min}^{(\text{jam})} = (g_{\max}^{(\text{jam})} + d)^{-1}$, $\rho_{\max} = d^{-1}$. The boundaries of a two-dimensional region for steady states of synchronized flow are: the upper line U determined by the condition $q = (1 - \rho d)/T_s$, the lower curve L determined by the condition $\rho G(q/\rho) = 1 - \rho d$, the curve (26) at $\rho \geq \rho_{\max}^{(\text{free})}$, and the vertical line $\rho = \rho_{\min}^{(\text{jam})}$.

3. Speed Adaptation Model

3.1. Empirical $F \rightarrow S \rightarrow J$ Transitions as Physical Basis of Speed Adaptation Model

The fundamental hypothesis of three-phase traffic theory, which postulates that hypothetical steady states of synchronized flow cover a two-dimensional region in the flow–density plane, is also one of the basic hypotheses of the ATD-model presented above (Fig. 1 (a, b)). In contrast with the ATD-model, in a speed adaptation model (**S**peed **A**daptation model, SA-model for short) presented below hypothetical steady states of synchronized flow are associated with a curve, i.e., they cover a one-dimensional region in the flow–density plane (curve S in Fig. 2 (a, b)). The curve S is associated with an averaging of an infinite number of steady states of synchronized flow to one synchronized flow speed for each space gap (density).

The basis hypothesis of the SA-model is associated with the sequence of $F \rightarrow S \rightarrow J$ transitions, which determine moving jam emergence in empirical observations [28, 7]. To explain the $F \rightarrow S \rightarrow J$ transitions, as in three-phase traffic theory in the SA-model it is assumed that at each given density in free flow the critical amplitude of a local fluctuation required for an $F \rightarrow S$ transition is considerably smaller than the one for an $F \rightarrow J$ transition.

Note that as in the models and theories in the context of the fundamental diagram approach [3, 4, 5, 6], in the SA-model steady state model solutions cover a one-dimensional region(s) in the flow–density plane. However, in the models and theories in the context of the fundamental diagram approach the $F \rightarrow J$ transition governs the onset of congestion [3, 4, 5, 6]. This is inconsequent with empirical results [7]. In contrast, in the SA-model the onset of congestion is associated with an $F \rightarrow S$ transition, whereas moving jams occur spontaneously only in synchronized flow, in accordance with empirical results.

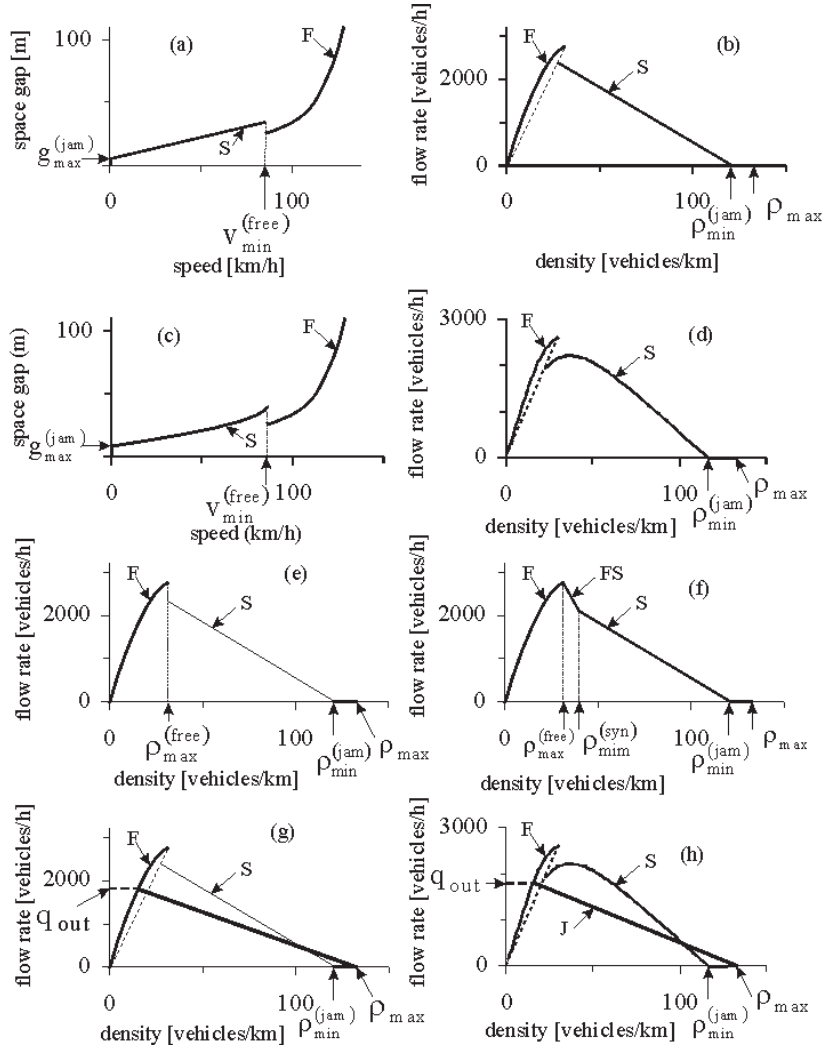


Figure 2. Model steady states for the SA-model: (a, b) - in the space-gap-speed (a) and the flow-density plane for the SA-model (27)–(33) (b). (c, d) - the SA-model (27)–(32), (34). (e, f) - other possible SA-models (see Appendix B). (g, h) - Steady states and the line J for the model (a, b) and the model (c, d).

The SA-model is simpler than the ATD-model. However, due to this simplification the SA-model cannot show some features of congested patterns of the ATD-model (Sect. 4.3), which are observed in empirical observations. The purpose of the SA-model is to simulate an F→S transition and features of the sequence of F→S→J transitions, as observed in empirical observations [28, 7], in a simple way. This confirms an assumption of three-phase traffic theory that if rather than the fundamental hypothesis of this theory, one of its consequences (e.g., the hypothesis about the F→S→J transitions, which is the basis of a mathematical model), then the model can show and predict some important empirical features of the phase transitions (see footnote 4 of Sect. 4.3.4 in [7]).

3.2. Basic Equations

There can be different possibilities for a separation of steady states of free flow and synchronized flow in SA-models, which all exhibit qualitatively the same features of the F→S→J transitions. To illustrate this, here we consider two variants of SA-models; in Appendix B two other possible variants of SA-models are discussed. All these variants of the SA-models exhibit very similar features of phase transitions and spatiotemporal congested traffic patterns that are associated with the same physics of these SA-models.

A formulation for the SA-model reads as follows

$$\frac{dx}{dt} = v, \quad (27)$$

$$\frac{dv}{dt} = \begin{cases} a^{(\text{free})} & \text{at } v \geq v_{\min}^{(\text{free})} \text{ and } g > g_{\max}^{(\text{jam})}, \\ a^{(\text{syn})} & \text{at } v < v_{\min}^{(\text{free})} \text{ and } g > g_{\max}^{(\text{jam})}, \\ a^{(\text{jam})} & \text{at } 0 \leq g \leq g_{\max}^{(\text{jam})}, \end{cases} \quad (28)$$

$a^{(\text{free})}$, $a^{(\text{syn})}$, and $a^{(\text{jam})}$ are vehicle accelerations (decelerations) in free flow, synchronized flow, and a wide moving jam, respectively; $v_{\min}^{(\text{free})}$ is the minimum speed in free flow associated with the maximum flow rate $q_{\max}^{(\text{free})}$ and the maximum density $\rho_{\max}^{(\text{free})}$ in accordance with the formula $v_{\min}^{(\text{free})} = q_{\max}^{(\text{free})} / \rho_{\max}^{(\text{free})}$. The vehicle acceleration $a = dv/dt$ in (28) is supposed to be limited by the maximum acceleration a_{\max} , i.e., in (28)

$$a^{(\text{phase})} = \min(\tilde{a}^{(\text{phase})}, a_{\max}), \quad (29)$$

where as above the superscript “phase” in (29) means either “free”, or “syn”, or else “jam”.

3.3. Vehicle Acceleration

Functions $\tilde{a}^{(\text{free})}(g, v, v_\ell)$, $\tilde{a}^{(\text{syn})}(g, v, v_\ell)$, and $\tilde{a}^{(\text{jam})}(v)$ in (29) are chosen as follows

$$\begin{aligned} \tilde{a}^{(\text{free})}(g, v, v_\ell) &= A^{(\text{free})}(V^{(\text{free})}(g) - v) + \\ &K^{(\text{free})}(v, v_\ell)(v_\ell - v), \end{aligned} \quad (30)$$

$$\begin{aligned} \tilde{a}^{(\text{syn})}(g, v, v_\ell) &= A^{(\text{syn})}(V_{\text{av}}^{(\text{syn})}(g) - v) + \\ &K^{(\text{syn})}(v, v_\ell)(v_\ell - v), \end{aligned} \quad (31)$$

$$\tilde{a}^{(\text{jam})}(v) = -K^{(\text{jam})}v. \quad (32)$$

Similarly to the ATD model, $V^{(\text{free})}(g)$ is a gap-dependent optimal speed in free flow; $V_{\text{av}}^{(\text{syn})}(g)$ is an average vehicle speed in steady states of synchronized flow; $A^{(\text{free})}$, $A^{(\text{syn})}$, $K^{(\text{free})}$, $K^{(\text{syn})}$, and $K^{(\text{jam})}$ are sensitivities.

Two versions of functions $V_{\text{av}}^{(\text{syn})}(g)$ in (31) that lead to two different versions of the SA-models are considered:

$$V_{\text{av}}^{(\text{syn})}(g) = \tilde{g}/T_{\text{av}}^{(\text{syn})}, \quad (33)$$

and

$$V_{\text{av}}^{(\text{syn})}(g) = V_1 \left[\tanh \left(\frac{\tilde{g}}{T_{\text{av}}^{(\text{syn})} V_1} \right) + c\tilde{g} \right], \quad (34)$$

where $\tilde{g} = g - g_{\text{max}}^{(\text{jam})}$; $T_{\text{av}}^{(\text{syn})}$, V_1 and c are constants.

3.4. Steady States and Model Parameters

In the SA-models, in accordance with (28) there are three isolated curves for steady states of the SA-models associated with the three traffic phases: free flow, synchronized flow, and wide moving jam (Fig. 2 (a, b)).

Steady states of free flow are related to a curve $v = V_{\text{F}}(\rho)$ given by (26) (the curve F in Fig. 2 (a-d)) associated with the condition

$$v = V^{(\text{free})}(g) \quad \text{at } v \geq v_{\text{min}}^{(\text{free})}. \quad (35)$$

Steady states of synchronized flow are related to a curve S in the space-gap-speed plane (Fig. 2 (a, c)) given by the condition

$$v = V_{\text{av}}^{(\text{syn})}(g) \quad \text{at } v < v_{\text{min}}^{(\text{free})} \text{ and } g > g_{\text{max}}^{(\text{jam})}. \quad (36)$$

In terms of the flow rate q and density ρ , the formula (36) reads

$$q = \rho V_{\text{S}}(\rho) \quad \text{at } \rho_{\text{min}}^{(\text{syn})} < \rho < \rho_{\text{min}}^{(\text{jam})}, \quad (37)$$

where $V_{\text{S}}(\rho) = V_{\text{av}}^{(\text{syn})}(g) |_{g=\rho^{-1}-d}$, $\rho_{\text{min}}^{(\text{syn})} = (g_{\text{max}}^{(\text{syn})} + d)^{-1}$, $g_{\text{max}}^{(\text{syn})}$ is found from the equation $V_{\text{av}}^{(\text{syn})}(g_{\text{max}}^{(\text{syn})}) = v_{\text{min}}^{(\text{free})}$.

In the case of the function $V_{\text{av}}^{(\text{syn})}(g)$ given by (33), the formula (37) yields the equation for the line S with a negative slope in the flow-density plane (Fig. 2 (b))

$$q = (1 - \rho/\rho_{\text{min}}^{(\text{jam})})/T_{\text{av}}^{(\text{syn})} \quad \text{at } \rho_{\text{min}}^{(\text{syn})} < \rho < \rho_{\text{min}}^{(\text{jam})}. \quad (38)$$

When the function $V_{\text{av}}^{(\text{syn})}(g)$ is given by formula (34), the curve S has a maximum in the flow-density plane (Fig. 2 (d)).

Steady states for a wide moving jam are the same as those in the ATD-model, i.e., they are given by a horizontal line

$$q = 0 \quad \text{at } \rho_{\text{min}}^{(\text{jam})} \leq \rho \leq \rho_{\text{max}} \quad (39)$$

in the flow-density plane (Fig. 2 (b, d)).

Parameters of the SA-model are shown in Table 3.

Table 3. SA-model parameters

| |
|---|
| $V^{(\text{free})}(g) = V(g),$ |
| $V(g) = V_0 \tanh(g/(V_0 T)), V_0 = 33.3 \text{ m/s (120 km/h)}, T = 0.85 \text{ s},$ |
| $a_{\text{max}} = 2 \text{ ms}^{-2}; A^{(\text{free})} = 0.4 \text{ s}^{-1},$ |
| $A^{(\text{syn})} = 0.1 \text{ s}^{-1}, K^{(\text{jam})} = 2 \text{ s}^{-1},$ |
| $K^{(\text{free})}(v, v_\ell) = K^{(\text{syn})}(v, v_\ell) = K(v, v_\ell)$ |
| where $K(v, v_\ell)$ is given in Table 1, |
| $K^{(\text{dec})}(v)$ is given in Table 1 at $v_c = 10 \text{ m/s}, \delta = 0.07.$ |
| In the SA model with function $V_{\text{av}}^{(\text{syn})}(g)$ (33), we use |
| $v_{\text{min}}^{(\text{free})} = 22.22 \text{ m/s (80 km/h)}, K_1^{(\text{dec})} = 0.95 \text{ s}^{-1} K_2^{(\text{dec})} = 0.64 \text{ s}^{-1},$ |
| $K^{(\text{acc})} = 0.4 \text{ s}^{-1}; T_{\text{av}}^{(\text{syn})} = 1.2 \text{ s}, g_{\text{max}}^{(\text{jam})} = 0.7 \text{ m}.$ |
| In the SA model with function $V_{\text{av}}^{(\text{syn})}(g)$ (34), we use |
| $v_{\text{min}}^{(\text{free})} = 23.61 \text{ m/s (85 km/h)}, K_1^{(\text{dec})} = 0.95 \text{ s}^{-1}, K_2^{(\text{dec})} = 0.75 \text{ s}^{-1},$ |
| $K^{(\text{acc})}(v) = 0.3 + 0.4 \min(1, v/12) \text{ s}^{-1}, V_1 = 20 \text{ m/s},$ |
| $c = 0.007 \text{ m}^{-1}, T_{\text{av}}^{(\text{syn})} = 1 \text{ s}, g_{\text{max}}^{(\text{jam})} = 1 \text{ m}.$ |

4. Diagram of Congested Traffic Patterns at On-Ramp Bottleneck

4.1. Congested Patterns in ATD-Model

Numerical simulations of the ATD-model show that a diagram of congested patterns (Fig. 3), which appear on the main road upstream of the bottleneck, is qualitatively the same as those for the stochastic model of Ref. [33, 34, 35]. The diagram (Fig. 3 (a)) shows regions of different types of congested patterns in the flow-flow plane whose co-ordinates are q_{on} and q_{in} .

There are two main boundaries in the diagram, $F_S^{(\text{B})}$ and $S_J^{(\text{B})}$ (Fig. 3 (a)). At the boundary $F_S^{(\text{B})}$, a first-order F→S transition occurs spontaneously leading to a synchronized flow pattern (SP) formation upstream of the bottleneck. At the boundary $S_J^{(\text{B})}$ in the diagram, wide moving jam(s) emerges spontaneously in synchronized flow upstream of the bottleneck, i.e., an S→J transition is realized. As a result, a general pattern (GP) emerges due to the sequence of the F→S→J transitions, if the flow rates q_{in} and q_{on} are related to a point $(q_{\text{on}}, q_{\text{in}})$ that is right of the boundary $S_J^{(\text{B})}$ in the diagram.

Depending on q_{in} and q_{on} , there are three types of SPs that can occur at the boundary $F_S^{(\text{B})}$ due to the F→S transition: A widening SP (WSP) (Fig. 3 (c)), a moving SP (MSP) (Fig. 3 (d)), and a localized SP (LSP) (Fig. 3 (e)); in addition in a neighborhood at the boundary $F_S^{(\text{B})}$ within the region of WSP in the diagram, an alternating SP (ASP) can occur (Fig. 3 (f)). These SPs exhibit qualitative features as those found in a stochastic three-phase traffic theory [33, 35].

If an WSP exists at the bottleneck (region labeled WSP & ASP in the diagram, Fig. 3 (a)) and at a given q_{in} the flow rate q_{on} gradually increases beyond the boundary $S_J^{(\text{B})}$ in the diagram, then wide moving jams begin to emerge spontaneously in synchronized flow of an initial WSP, i.e., the WSP transforms into one of the GPs.

There are two possibilities for GP formation right of the boundary $S_J^{(\text{B})}$: (i) At greater flow rates q_{in} , a dissolving GP (DGP) appears (Fig. 3 (h)), if a point

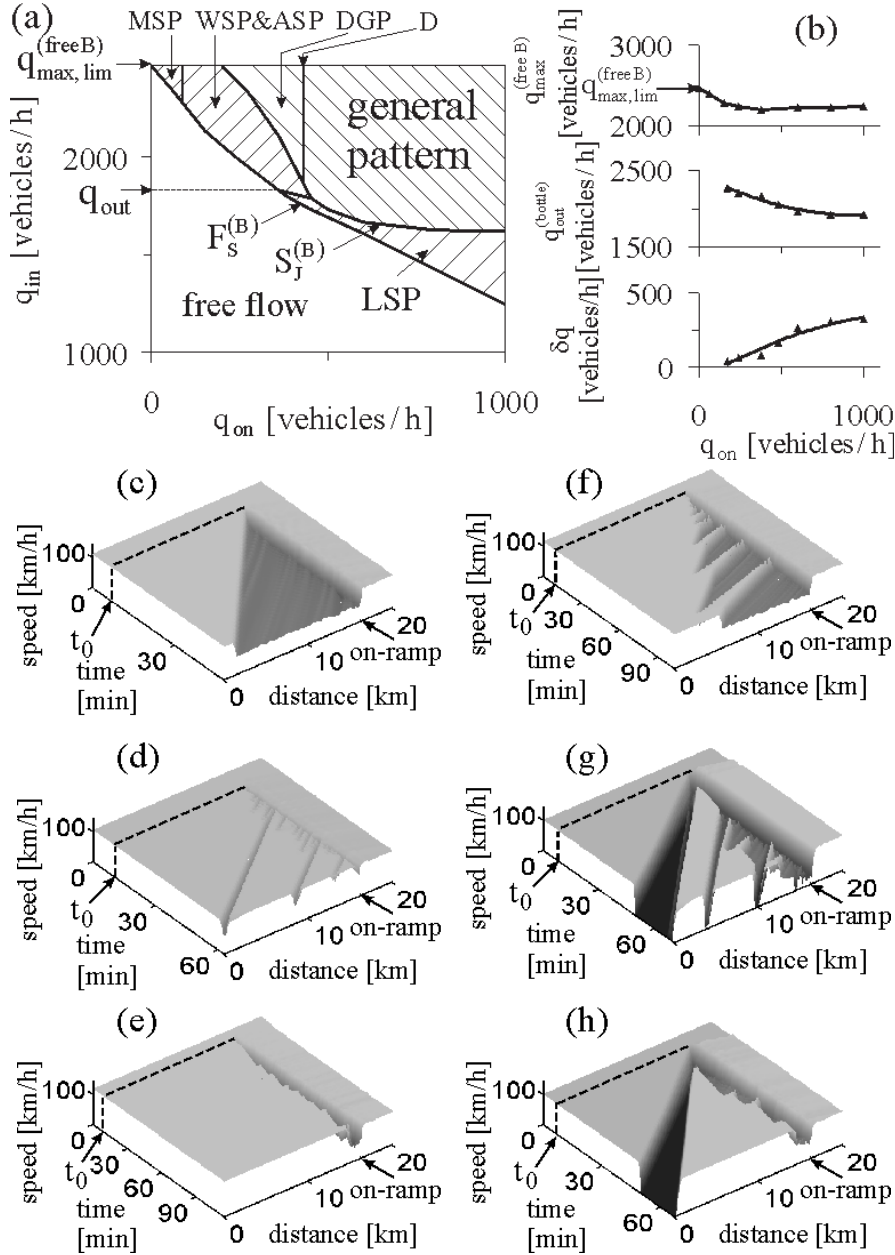


Figure 3. Congested patterns in the ATD-model: (a) – Diagram of congested patterns. (b) – Maximum capacity in free flow at the bottleneck $q_{max,lim}^{(free B)}$, the discharge flow rate downstream of the congested bottleneck $q_{out}^{(bottle)}$, and the capacity drop δq . (c–h) – Congested patterns upstream of the bottleneck related to (a): (c–f) – SPs and (g, h) – GPs. (c) – WSP, (d) – sequence of MSPs, (e) – LSP, (f) – alternating synchronized flow pattern (ASP), (g) – GP, (h) – DGP. In (c–f) the flow rates (q_{on}, q_{in}) are: (c) (350, 2140), (d) (60, 2340), (e) (360, 1800), (f) (240, 2026), (g) (460, 2450), (h) (360, 2450) vehicles/h. $q_{max,lim}^{(free B)} \approx 2470$ vehicles/h. In (b) the discharge flow rate $q_{out}^{(bottle)}$ is changed from 2270 vehicles/h to 1925 vehicles/h, $q_{out} \approx 1805$ vehicles/h.

$(q_{\text{on}}, q_{\text{in}})$ is within the region labeled DGP in the diagram. (ii) At smaller q_{in} right of the boundary $S_J^{(\text{B})}$, an initial SP (WSP or LSP) transforms into an GP in which no interruption of wide moving jam emergence in synchronized flow is realized (Fig. 3 (g)). Such GPs appears also at greater q_{in} right of the line D in the diagram.

As in the KKW cellular automata (CA) model [34, 7], in the ATD-model the maximum flow rate in free flow downstream of the bottleneck $q_{\text{max}}^{(\text{free B})}$ is a decreasing function of q_{on} (Fig. 3 (b)). Recall, that the flow rate $q_{\text{max}}^{(\text{free B})}(q_{\text{on}})$ is the flow rate associated with the boundary $F_S^{(\text{B})}$ in the diagram of congested patterns at which an F→S transition occurs at the bottleneck. After a congested pattern is formed at the bottleneck due to this F→S transition, the flow rate downstream of the congested bottleneck called discharge flow rate $q_{\text{out}}^{(\text{bottle})}$ (Fig. 3 (b)) is usually smaller than the initial flow rate $q_{\text{max}}^{(\text{free B})}$. The difference

$$\delta q(q_{\text{on}}) = q_{\text{max}}^{(\text{free B})}(q_{\text{on}}) - q_{\text{out}}^{(\text{bottle})}(q_{\text{on}}) \quad (40)$$

called ‘‘capacity drop’’ (see references in [7]) is an increasing function of q_{on} at the boundary $F_S^{(\text{B})}$ in the diagram of congested patterns.

4.2. Nucleation and Metastability Effects of Pattern Formation

Numerical simulations show that an F→S transition at the bottleneck is a first-order phase transition, which is accompanied by nucleation and metastability effects, as well as by a hysteresis in SP emergence and dissolution. If an initial point $(q_{\text{on}}, q_{\text{in}})$ is left of the boundary $F_S^{(\text{B})}$ in the diagram (Fig. 3 (a)), there is a limited region in the diagram in which a short-time local speed (density) perturbation in a neighborhood of the bottleneck can lead to an induced F→S transition at the bottleneck. At a greater perturbation, after an F→S transition has occurred at the bottleneck, wide moving jams emerge spontaneously in synchronized flow, i.e., an GP is induced.

These nucleation and metastability effects are characteristic for both ATD- and SA-models. For simplicity, we restrict their consideration to the SA-model (27)–(33) (Figs. 4 and 5). When an initial state at the bottleneck is free flow in which q_{in} is given and q_{on} increases gradually, then a speed (density) perturbation in free flow localized at the bottleneck appears spontaneously. The perturbation consists of deterministic and random components. The random component is associated with different dynamic behavior of vehicles merging onto the main road from the on-ramp. The deterministic component (deterministic perturbation for short) is permanent and motionless. This is because the deterministic perturbation is caused by merging of two flows with the flow rates q_{in} and q_{on} within freeway locations associated with the merging region of the bottleneck. A spatial dependence of speed and density within the deterministic perturbation localized in the merging region of the on-ramp (labeled ‘‘on-ramp’’ in Fig. 4 (a, b)) can be approximately found by averaging of space functions of speed and density over long enough time interval (Fig. 4 (a, b)).

As the deterministic perturbation at given q_{in} and q_{on} is motionless, the total flow rate (across the main road and on-ramp lane) $q_{\text{sum}} = q_{\text{in}} + q_{\text{on}}$ within the perturbation does not depend on spatial co-ordinate, whereas the speed $v(x)$ and density $\rho(x)$ change in free flow at the bottleneck: $q_{\text{sum}} = v_{\text{free}}^{(\text{B})}\rho_{\text{free}}^{(\text{B})} = v^{(\text{free})}\rho^{(\text{free})}$, where $v_{\text{free}}^{(\text{B})}$ and $\rho_{\text{free}}^{(\text{B})}$ are the minimum speed and maximum density within the perturbation; $v^{(\text{free})}$, $\rho^{(\text{free})}$ the speed and density downstream of the perturbation (Fig. 4 (a, b)); $v_{\text{free}}^{(\text{B})} < v^{(\text{free})}$, $\rho_{\text{free}}^{(\text{B})} > \rho^{(\text{free})}$.

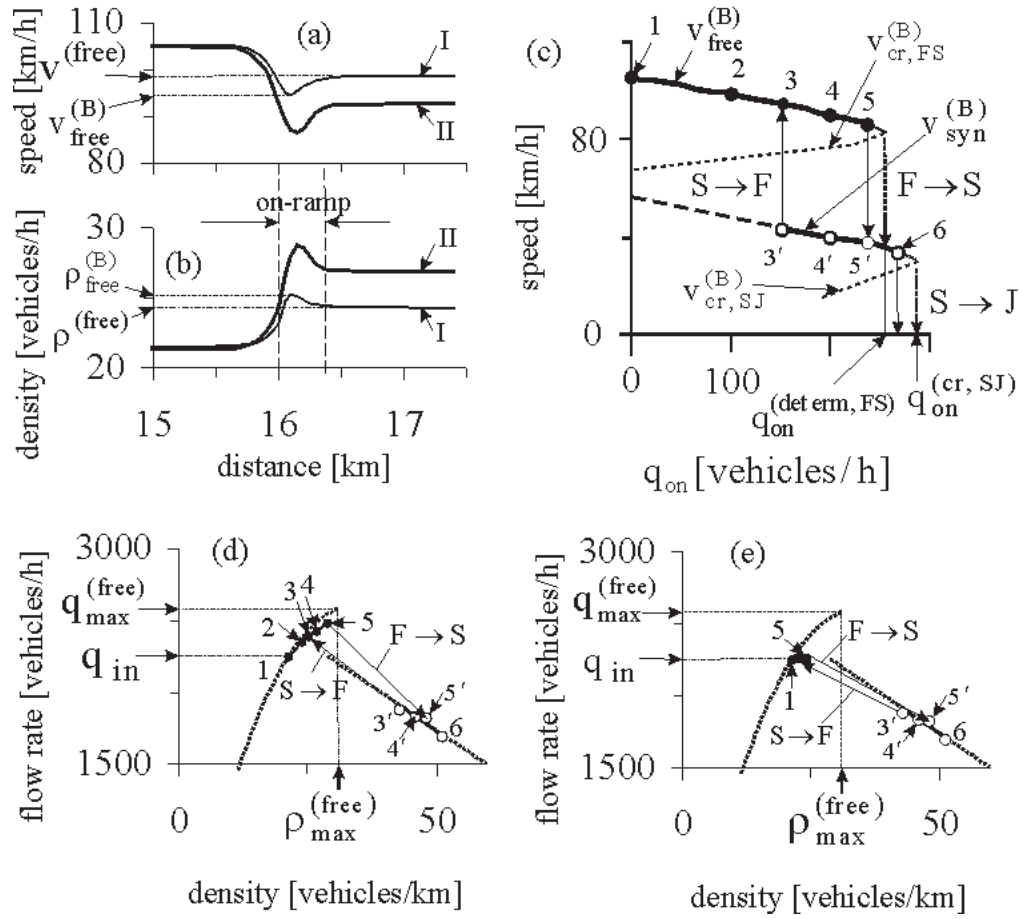


Figure 4. Nucleation and metastability of free flow and synchronized flow in the SA-model: (a, b) – Spatial dependence of the speed (a) and density (b) within the deterministic perturbation in free flow at the bottleneck for two flow rates $q_{on} = 150$ (curve I) and 240 (curve II) vehicles/h at $q_{in} = 2252$ vehicles/h. (c) – Double Z-characteristic in the flow-rate–speed plane for the sequence of $F \rightarrow S \rightarrow J$ transitions. (d, e) – Hysteresis effects in the flow–density plane due to $F \rightarrow S$ and reverse $S \rightarrow F$ transitions. Dotted curves in (d, e) are related to steady state model solutions.

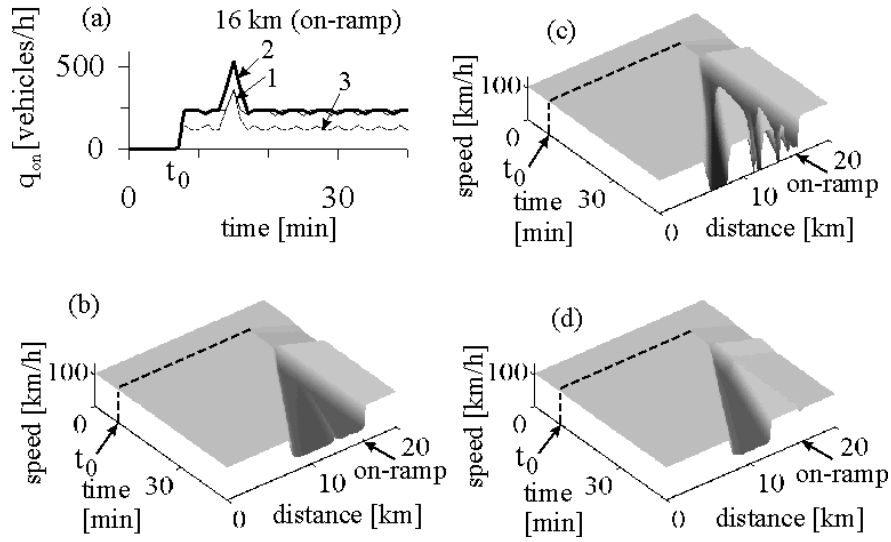


Figure 5. Congested pattern excitation in metastable free flow: (a) – Short-time (2 min) perturbations in the flow rate q_{on} used for pattern excitation. (b–d) – WSP (b), GP (c), and MSP (d) induced by the related perturbations (curve 1, 2, and 3 in (a), respectively). $q_{in} = 2252$ vehicles/h. $q_{on} = 220$ vehicles/h in (b, c) and $q_{on} = 140$ vehicles/h in (d). Amplitudes of perturbations in (a) are: 270 vehicles/h for (b, d) and 500 vehicles/h for (c).

The speed $v_{\text{free}}^{(B)}$ decreases when q_{on} increases (from point 1 to 5 in Fig. 4 (c)). Consequently, $\rho_{\text{free}}^{(B)}$ increases. In the flow–density plane, the flow rate on the main road associated with this density increases too (from point 1 to 5 in Fig. 4 (d)), whereas the flow rate upstream of the perturbation is equal to q_{in} , i.e., it does not change (from point 1 to 5 in Fig. 4 (e)). This increase in the perturbation amplitude with q_{on} has a limit $q_{\text{on}} = q_{\text{on}}^{(\text{determ., FS})}$ associated with the deterministic F→S transition (dotted down-arrow in Fig. 4 (c)). However, non-homogeneous free flow dynamics, which is caused by vehicle merging, results in an F→S transition at a smaller q_{on} (point 5 in Fig. 4 (c)) related to a point on the boundary $F_S^{(B)}$ in the diagram of congested patterns (Fig. 6 (a)). The speed decreases and density increases abruptly within the initial perturbation (arrows F→S from point 5 to 5' in Fig. 4 (c–e)) and a congested pattern emerges at the bottleneck. In the example, an WSP occurs upstream of the bottleneck due to the F→S transition.

If now q_{on} decreases, the speed within the WSP increases (from point 5' to 3' in Fig. 4 (c–e)). This synchronized flow speed increase also has a limit: The speed increases and density decreases abruptly within the synchronized flow (arrows S→F from the point 3' to 3 in Fig. 4 (c–e)) and free flow returns at the bottleneck.

However, at the chosen model parameters, this free flow can persist for a short time only: A new F→S transition occurs spontaneously and MSPs emerge at the bottleneck (dashed part of the synchronized flow states $v_{\text{syn}}^{(B)}$ in Fig. 4 (c)). This is because the threshold flow rate q_{th} for MSP existence is smaller than a chosen value q_{in} . Thus, in accordance with stochastic models [35] at $q_{\text{on}} > 0$ an MSP(s) emerges spontaneously at the bottleneck. Even if $q_{\text{on}} = 0$, an MSP can be induced by application a short-time local perturbation in free flow with $q_{\text{in}} > q_{\text{th}}$. The amplitude of this perturbation should be greater than the critical amplitude associated with the critical branch on the Z-characteristic $v_{\text{cr, FS}}^{(B)}$. This Z-characteristic for the F→S and reverse S→F transitions at the bottleneck consists of the states for free flow associated with the deterministic perturbation at the bottleneck $v_{\text{syn}}^{(B)}$, the critical branch $v_{\text{cr, FS}}^{(B)}$, and synchronized flow states $v_{\text{syn}}^{(B)}$ (Fig. 4 (c)). In accordance with this Z-characteristic, we get the associated hysteresis effects on the fundamental diagram (arrows F→S and S→F in Fig. 4 (d, e)).

If in contrast q_{on} increases, the speed within the WSP decreases (Fig. 4 (c)). This speed decrease has a limit associated with the flow rate $q_{\text{on}} = q_{\text{on}}^{(\text{cr, SJ})}$ at which an S→J transition must occur (dotted down-arrow S→J in Fig. 4 (c)). However, because there are speed and density waves of a finite amplitude in synchronized flow, an S→J transition occurs already for $q_{\text{on}} < q_{\text{on}}^{(\text{cr, SJ})}$ (point 6 and solid down-arrow in Fig. 4 (c)). As a result, an GP emerges. This is because in the ATD- and SA-models, synchronized flow states that are above the line J in the flow–density plane are metastable ones against wide moving jam emergence. This can be seen from another Z-characteristic in the flow–rate–speed plane for an S→J transition in synchronized flow that consists of the states for synchronized flow $v_{\text{syn}}^{(B)}$, the critical branch for critical perturbations in synchronized flow $v_{\text{cr, SJ}}^{(B)}$, and the line $v = 0$ for wide moving jams (Fig. 4 (c)).

From the resulting double Z-characteristic, it can be concluded that in a metastable free flow at the bottleneck (left of the boundary $F_S^{(B)}$ in the diagram in Fig. 6 (a)) depending on amplitude of a time-limited perturbation caused, for example, by an increase in q_{on} (curves 1 and 2 in Fig. 5 (a)), either an WSP (Fig. 5 (b)) or an GP (Fig. 5 (c)) can be induced. At smaller q_{on} (curve 3 in Fig. 5 (a)), an MSP (Fig. 5 (d))

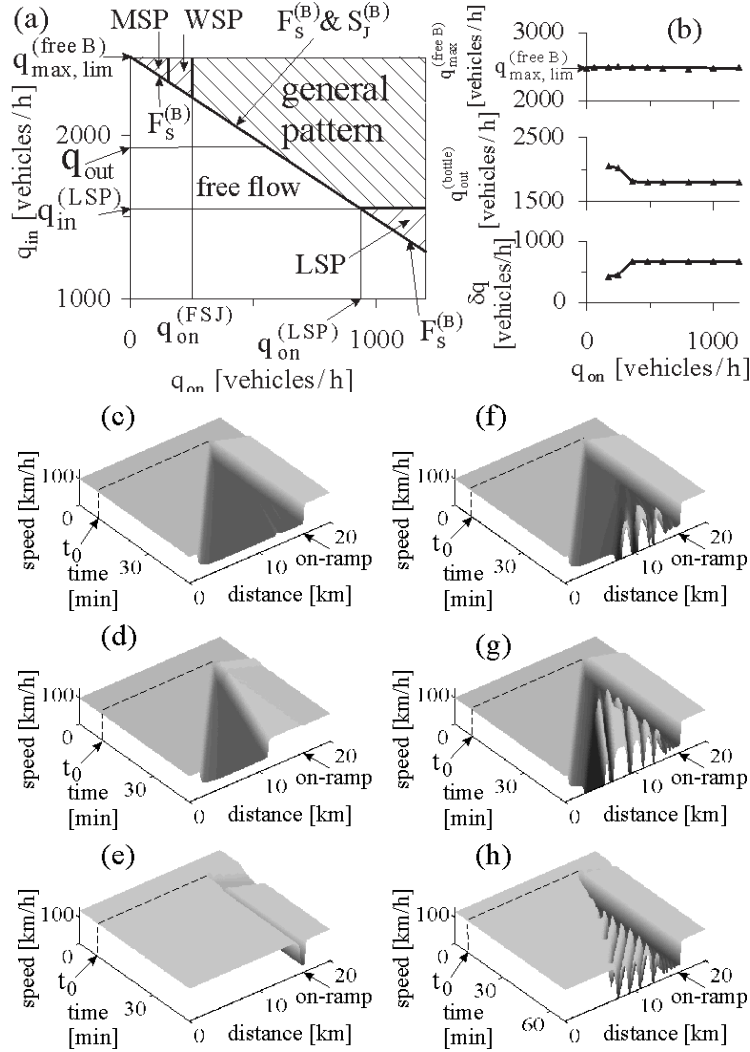


Figure 6. Diagram of congested patterns at the on-ramp bottleneck in SA-model (28), (33) (a), maximum capacity in free flow at the bottleneck (b) and congested patterns (c-h) related to (a): (c-e) – SPs and (f-h) – GPs. (c) – WSP, (d) – MSP, (e) – LSP, (f) – GP arising from WSP at smaller q_{on} , (g) – GP at $q_{in} > q_{out}$, (h) – GP at $q_{in} < q_{out}$. In (c-h) the flow rates (q_{on}, q_{in}) are: (c) (200, 2353), (d) (140, 2378), (e) (940, 1520), (f) (250, 2353), (g) (400, 2353), and (h) (900, 1770) vehicles/h. $q_{max,lim}^{(free B)} \approx 2475$ vehicles/h.

can be excited in free flow. All results presented in Figs. 4 and 5 for the SA-model remain qualitatively equal for the ATD-model.

4.3. Congested Patterns in SA-Models

The SA-model (28), (33) (Fig. 6) exhibits the following shortcoming in comparison with the ATD-model (Fig. 3):

(i) If the flow rate q_{on} is within a flow rate range $q_{\text{on}}^{(\text{FSJ})} < q_{\text{on}} < q_{\text{on}}^{(\text{LSP})}$, then no SP can be formed at the boundary $F_S^{(\text{B})}$ in the diagram (Fig. 6 (a)): The sequence of $F \rightarrow S \rightarrow J$ transitions occurs spontaneously at this boundary, leading to GP emergence. For this reason, the related part of the boundary at which GPs emerge spontaneously in free flow at the bottleneck is labeled $F_S^{(\text{B})}$ & $S_J^{(\text{B})}$.

(ii) If the flow rate q_{in} at this boundary decreases, another characteristic flow rate $q_{\text{in}} = q_{\text{in}}^{(\text{LSP})}$ associated with the flow rate $q_{\text{on}} = q_{\text{on}}^{(\text{LSP})}$ at this boundary is reached: At $q_{\text{in}} < q_{\text{in}}^{(\text{LSP})}$ all moving jams that emerge in synchronized flow upstream of the bottleneck dissolve. As a result, at $q_{\text{in}} < q_{\text{in}}^{(\text{LSP})}$ and right of the boundary $F_S^{(\text{B})}$ only an LSP remains at the bottleneck. Within this LSP the speed is very low. This LSP has a qualitative different nature in comparison with an LSP of higher synchronized flow speed in the ATD-model that occurs at considerably greater q_{in} (Fig. 3).

(iii) In contrast with the ATD-model and with empirical observations, in the SA-model synchronized flow cannot be formed in wide moving jam outflow, i.e., only free flow occurs in the wide moving jam outflow. The reason for this is as follows. To simulate moving jam emergence in synchronized flow, the average branch for synchronized flow $V_{\text{av}}^{(\text{syn})}$ lies for higher speeds above the line J (Fig. 2 (g)). Flow states in the jam outflow should be related to points on the line J . However, all synchronized flow states at higher speeds are above the line J . Thus, there are no synchronized flow states in the jam outflow. This explains why only free flow can be formed in the jam outflow in the SA-model. ||

The mentioned shortcoming of the SA-model result from the averaging of a 2D-region of steady states for synchronized flow in the flow–density plane of the ATD-model (Fig. 1 (a)) to the branch for average synchronized flow states $V_{\text{av}}^{(\text{syn})}$ in Fig. 2.

If the branch for average synchronized flow states $V_{\text{av}}^{(\text{syn})}$ in a SA-model has a part with a positive slope (Fig. 2 (d)), then LSPs of higher speeds appear in the diagram of congested patterns (Fig. 7). However, these LSPs should be considered a model effect only, rather than they are related to LSPs observed in empirical observations. To explain this, note that these model LSPs are very narrow ones (Fig. 7 (e)). They are localized within the merging region of the on-ramp and consist of two narrow fronts only (Fig. 8 (a)): There is no region of synchronized flow between the fronts within these LSPs. This is regardless of the flow rates q_{in} and q_{on} . The downstream front of an LSP is associated with a drop in the speed (and jump in density) due to a transition from a free flow state on the curve F to an average synchronized flow state on the part of the branch $V_{\text{av}}^{(\text{syn})}$ with a positive slope (curve S in Fig. 2 (d)).

|| The only exclusion is the SA-model with the function $V_{\text{av}}^{(\text{syn})}$ (34), if parameters for the curve S and/or the line J , i.e., for wide moving jam propagation are chosen different as those shown in Fig. 2 (c, d, h): These different parameters should lead to an intersection of the line J with the branch of the curve $V_{\text{av}}^{(\text{syn})}$ with a positive slope in the flow–density plane. However, in this specific case only synchronized flow associated with the point of the latter intersection can appear in the moving jam outflow, i.e., this is also a model effect.

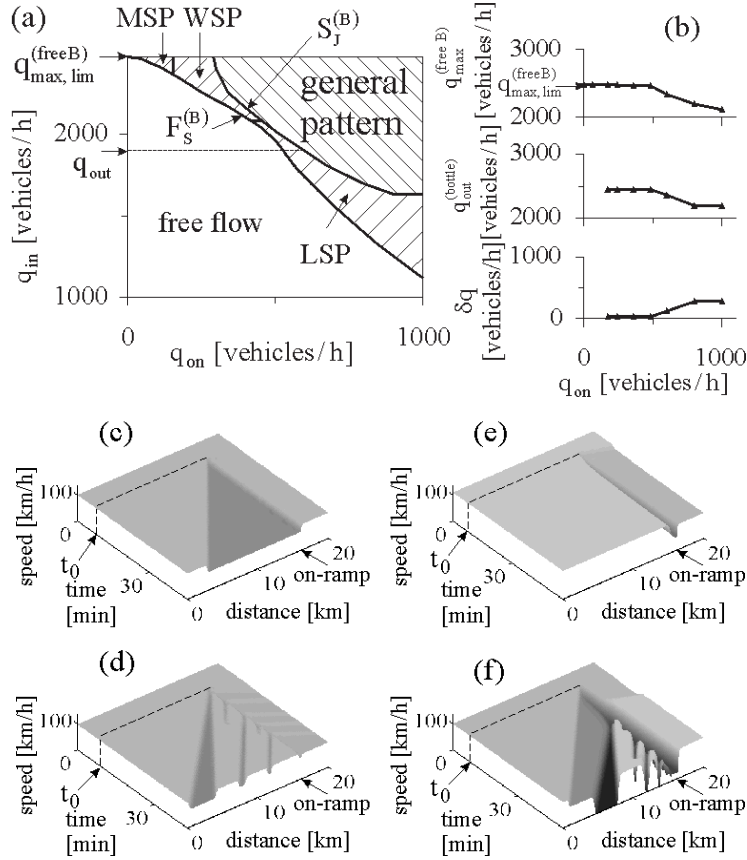


Figure 7. Diagram of congested patterns at the on-ramp bottleneck in the SA-model (28), (34) (a), the capacity in free flow $q_{max}^{(free B)}$, the discharge flow rate at the on-ramp $q_{out}^{(bottle)}$ and the capacity drop δq (b), and congested patterns (c-f) related to (a): (c-e) - SP and (f) - GP. (c) - WSP, (d) - subsequence of MSP, (e) - LSP, (f) - GP arising from WSP. In (c-f) the flow rates (q_{on}, q_{in}) are: (c) (200, 2400), (d) (90, 2450), (e) (360, 2115), (f) (300, 2400) vehicles/h. In the model $q_{max, lim}^{(free B)} \approx 2475$ vehicles/h. In (b) the discharge flow rate $q_{out}^{(bottle)}$ is changed from 2450 vehicles/h to 2200 vehicles/h, $q_{out} \approx 1880$ vehicles/h.

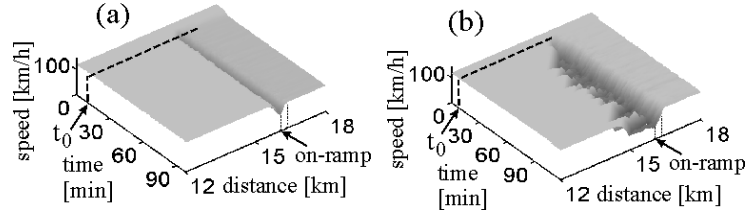


Figure 8. Comparison of LSPs in the SA-model with the function $V_{av}^{(syn)}$ (34) (a) and in the ATD-model (b). The LSPs and their parameters are the same as those in Fig. 7 (e) and, Fig. 3 (e) respectively.

The upstream front of the LSP is associated with a reverse transition (Fig. 8 (a)). Conflictingly, in empirical observations rather than such narrow LSPs, an extended region of synchronized flow is usually observed within an empirical LSP and the LSP width changes over time considerably. These empirical features of LSPs shown by the ATD-model (Fig. 8 (b)) are not found in the SA-model.

At chosen SA-model parameters the condition

$$q_{out} > q^{(pinch)} \quad (41)$$

is satisfied, where $q^{(pinch)}$ is the flow rate within the pinch region of an GP in which narrow moving jams emerge. Under the condition (41), no DGPs appear in the SA-

models (Figs. 6 and 7). At other parameters of the SA-models, an opposite condition

$$q_{\text{out}} < q^{(\text{pinch})} \quad (42)$$

can be satisfied. Then DGPs appear in the SA-models.

The maximum flow rate in free flow downstream of the bottleneck $q_{\text{max}}^{(\text{free B})}(q_{\text{on}})$, the discharge flow rate $q_{\text{out}}^{(\text{bottle})}$, and the ‘‘capacity drop’’ δq can sometimes exhibit different features as those in the ATD-model (Fig. 3 (b)) when the flow rate q_{on} changes (Figs. 6 (b) and 7 (b)). Particularly, in contrast with the ATD-model, in the SA-model (28), (33) $q_{\text{max}}^{(\text{free B})}$ does not depend on q_{on} , whereas in the SA-model (28), (34) $q_{\text{max}}^{(\text{free B})}$ depends on q_{on} but at considerably greater q_{on} than for the ATD-model.

Simulations show that the SA models presented in Appendix B show qualitatively the same features of the phase transitions and spatiotemporal congested patterns as those in the SA-model (28), (33).

4.4. Comparison with Stochastic SA-Models

As mentioned in Sect. 4.1, the ATD-model, in which a 2D region of synchronized flow steady states is used, exhibits many similar features of the stochastic microscopic model with a 2D region of synchronized flow steady states first introduced in [33] and further developed in [35]. It is interesting to compare the deterministic SA-models introduced in this article with possible *stochastic* SA-models. Such models can be derived from the stochastic model of Ref. [33, 35], if 2D region of synchronized flow steady states is averaged to synchronized flow states related to a 1D region in the flow–density plane.

A stochastic SA-model can easily be derived from the stochastic model of Ref. [35] based on the physics and ideas for the SA-model approach discussed in Sect. 3. To reach this goal, in the dynamic part of the stochastic model of Ref. [35]

$$v_{n+1} = \max(0, \min(v_{\text{free}}, v_{c,n}, v_{s,n})), \quad (43)$$

$$x_{n+1} = x_n + v_{n+1}\tau \quad (44)$$

for a desired speed in synchronized flow $v_{c,n}$, rather than the formula (3) of Ref. [35] leading to a 2D region of synchronized flow steady states in the flow–density plane, the following equations associated with the physics of the SA-models of Sect. 3 are used:

$$v_{c,n} = v_n + \max(-b_n\tau, \min(a_n\tau, \Delta_n)), \quad (45)$$

$$\Delta_n = \begin{cases} A^{(\text{free})}(g_n)(v_{\text{free}} - v_n) + \\ K^{(\text{free})}(v_{\ell,n} - v_n) & \text{at } g \geq g_{\text{min}}^{(\text{free})}, \\ A^{(\text{syn})}(V_{\text{av}}^{(\text{syn})}(g_n) - v_n) \\ + K^{(\text{syn})}(v_{\ell,n} - v_n) & \text{at } g < g_{\text{min}}^{(\text{free})}. \end{cases} \quad (46)$$

In (43)–(46), v_n and x_n are the speed and space co-ordinate of a vehicle; the index n corresponds to the discrete time $t = n\tau$, $n = 0, 1, 2, \dots$; τ is the time step; v_{free} is the maximum speed in free flow which is considered as a constant value; $v_{s,n}$ is the save speed of Ref. [35]; the lower index ℓ marks variables related to the preceding vehicle; all vehicles have the same length d ; $a_n \geq 0$ is acceleration, $b_n \geq 0$ is deceleration; the space gap $g_n = x_{\ell,n} - x_n - d$; the average speed in synchronized flow steady states $V_{\text{av}}^{(\text{syn})}$ is given by the formula (33) at $g_{\text{max}}^{(\text{jam})} = 0$. Of course, other formulations for the

average synchronized flow steady states $V_{\text{av}}^{(\text{syn})}$, for example used in the deterministic SA-models (Fig. 2 (b, d, f)) can also be applied.

In general, descriptions of random vehicle acceleration and deceleration are the same as those in the stochastic model of Ref. [33, 35]: At the first step, the preliminary speed \tilde{v}_{n+1} is set to $\tilde{v}_{n+1} = v_{n+1}$ where the speed v_{n+1} is calculated from the dynamic equations (43)–(46). At the second step, a noise component ξ_n is added to the calculated speed \tilde{v}_{n+1} . Then the final speed is found from the condition [35]

$$v_{n+1} = \max(0, \min(v_{\text{free}}, \tilde{v}_{n+1} + \xi_n, v_n + a_{\text{max}}\tau, v_{\text{s,n}})), \quad (47)$$

where a_{max} is the maximum acceleration.

However, in contrast with the stochastic model of Ref. [35], the noise component ξ_n in (47) can be different from zero *only*, if the vehicle decelerates, specifically

$$\xi_n = \begin{cases} -b_{\text{max}}\tau\theta(p_b - r) & \text{if } \tilde{v}_{n+1} < v_n - \delta \\ 0 & \text{otherwise,} \end{cases} \quad (48)$$

where $r = \text{rand}(0, 1)$, $\theta(z) = 0$ at $z < 0$ and $\theta(z) = 1$ at $z \geq 0$, $\delta \ll 1$, b_{max} , p_b are constants. The acceleration a_n and deceleration b_n in (46) are taken as the same stochastic functions as those in the model of Ref. [35].

Simulations show that the stochastic SA-model (43)–(48) exhibits qualitatively similar features of phase transitions and of spatiotemporal congested patterns at the on-ramp bottleneck (Fig. 9) as those in the associated deterministic SA-models (Fig. 6). Note that under the chosen model parameters in the stochastic SA-model (43)–(48) the condition (42) is satisfied. As a result, there is a region in the diagram of congested patterns in which DGPs occur (region labeled DGP in Fig. 9 (a)). After the wide moving jam of the DGP is upstream of the bottleneck as well as in the ATD-model, an LSP remains at the bottleneck (Fig. 9 (h)). In contrast with the ATD-model, this LSP exists for a finite time interval only and free flow finally emerging at the bottleneck. However, in a small neighborhood of the boundary labeled D in the diagram, which separates DGPs and GPs, there is a peculiarity in pattern formation, which is related to all deterministic SA-models under the condition (42): If the flow rate q_{on} increases in the neighborhood of the boundary D in the diagram, then the lifetime of an LSP, which occurs within an DGP increases and it tends towards infinity at the boundary D (Fig. 10 (a)). This quasi-steady LSP is explained by a very long interval between wide moving jam emergence in the synchronized flow at the bottleneck, which tends towards infinity at the boundary D. Indeed, already a very small increase in q_{on} beyond the boundary D leads to GP formation with a long interval between wide moving jams (Fig. 10 (b)).

5. Discussion

5.1. Comparison of ATD- and SA-models with OV-models and other Deterministic Models

The first term in the formula for vehicle acceleration $a^{(\text{free})}$ (9), $A(g, v)(V(g) - v)$, describes the dynamics of the vehicle speed v in the free flow phase in the vicinity of the optimal speed in free flow $V(g)$. At a time scale that is considerably greater than the time delay τ , this dynamic behavior is the same as those in different OV-models [3, 4, 5, 22], which can be written as follows

$$\frac{dv}{dt} = A(g, v)(V(g) - v). \quad (49)$$

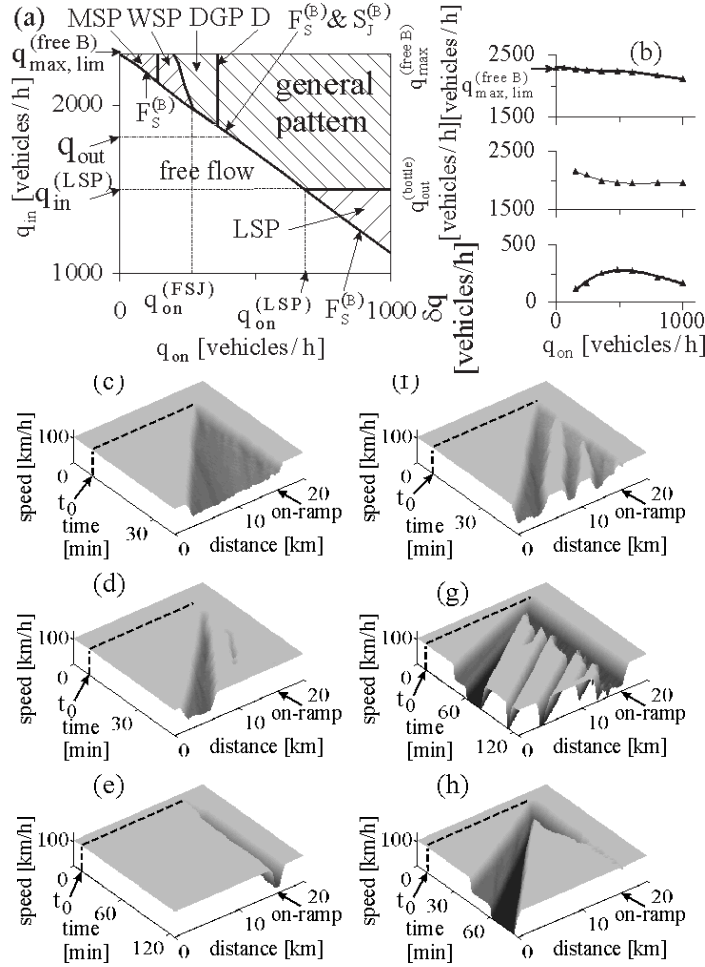


Figure 9. Diagram of congested patterns at the on-ramp bottleneck in the stochastic SA-model (43)–(48) (a), maximum capacity in free flow at the bottleneck (b) and congested patterns (c–h) related to (a): (c–f) – SPs and (g, h) – GPs. (c) – WSP, (d) – MSP, (e) – LSP, (f) – ASP, (g) – GP, (h) – DGP. In (c–h) the flow rates (q_{on}, q_{in}) are: (c) (200, 2250), (d) (60, 2250), (e) (720, 1470), (f) (120, 2235), (g) (500, 2220), and (h) (352, 2235) vehicles/h. $q_{max, lim}^{(free B)} \approx 2300$ vehicles/h. Model parameters: $A^{(free)}(g_n) = 0.5 \min(1, (g_n - g_{min}^{(free)})/20)$, $g_{min}^{(free)} = 36$ m, $A^{(syn)} = 0.1$, $T_{av}^{(syn)} = 1.45$ s, $g_{max}^{(jam)} = 0$, $p_b = 0.02$, $p_1 = 0.55$, $p_2(v_n) = 0.5 + 0.48\theta(v_n - 15)$, $a_{max} = b_{max} = 0.5$ m/s². The other parameters are the same as those in [35]. The on-ramp model from [35, 36] is used, in which the synchronization gaps $G_n^+ = G_n^- = g_{min}^{(free)}$.

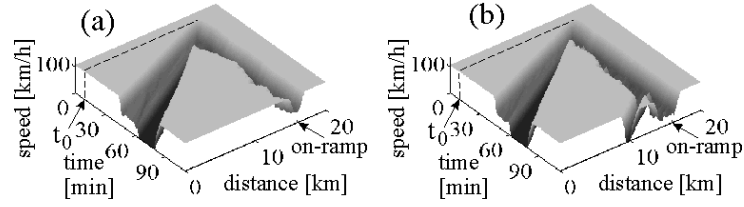


Figure 10. Transformation of DGP in Fig. 9 (h) to GP with a very long time interval between wide moving jam emergence (b) through an DGP with a quasi-steady LSP (a) by a small increase in the flow rate (q_{on} in a neighborhood of the boundary D in the diagram of congested patterns in Fig. 9 (a)). The flow rates (q_{on}, q_{in}) are: (a) (357, 2235) and (b) (362, 2235) vehicles/h.

However, in the OV-models the vehicle acceleration $A(g, v)(V(g) - v)$ is valid for the whole possible space gap range [3, 4, 5, 22]

$$g \geq 0. \tag{50}$$

In contrast with the OV-models, in the ATD-model this vehicle acceleration is applied for large space gaps

$$g > G \tag{51}$$

associated with free flow *only*.

The crucial difference of the ATD-model with the OV-models and all other deterministic microscopic traffic flow models (see references in the reviews [1, 3, 4, 5, 6]) is that the vehicle acceleration behavior qualitatively changes when the vehicle is within the synchronization gap, i.e., if the condition

$$g \leq G, \quad (52)$$

which is opposite to the condition (51), is satisfied.

The condition (52) is associated with the synchronized flow phase in which there is *no* optimal speed in the ATD-model. This conclusion follows from (10) and its analysis made in Sect. 2.6 in which it has been shown that for a given steady space gap in synchronized flow there are an infinity of steady vehicle speeds within a finite speed range (Fig. 1 (a)).

The crucial differences between the SA-models and OV-models and all other deterministic microscopic traffic flow models in which steady states covering a one-dimensional region(s) in the flow–density plane (see references in the reviews [1, 3, 4, 5, 6]) are as follows. In the SA-models, at each density of free flow states the critical amplitude of a local perturbation required for an F→S transition is considerably smaller than the critical amplitude of a local perturbation required for an F→J transition.

In the SA-models, there are two ranges of model steady states separated one from another by a model discontinuity in vehicle space gap or in speed (Fig. 2 (a–e)) or else due to instability of model steady states against infinitesimal non-homogeneous fluctuations (Fig. 2 (f)) This simulates the hypothesis of three-phase traffic theory about a competition between over-acceleration and speed adaptation effect that is responsible for F→S and S→F transitions: The first range of steady states simulates free flow, whereas the second simulates synchronized flow. To simulate S→J transitions within synchronized flow, steady states associated with synchronized flow are metastable with respect to moving jam emergence, i.e., moving jams emerge in these synchronized flow states *only* if large enough amplitude local perturbations appear. These requirements to the SA-models lead to F→S→J transitions that are responsible for moving jam emergence found in empirical data [7].

5.2. Critical Discussion of Theories and Models based on the Fundamental Diagram Approach

In the OV model (49), as in other deterministic (and stochastic) traffic flow models in the context of the fundamental diagram approach, which claim to show spontaneous jam emergence, there is a range of the density on the fundamental diagram in which steady states on this diagram are unstable against infinitesimal perturbations [3, 4, 5, 6]. This instability leads to wide moving jam emergence in these models both on homogeneous road and at a bottleneck, i.e., to an F→J transition. We denote the minimum density of this density range, in which infinitesimal fluctuations grow, by $\rho_{\text{cr}}^{(\text{FJ})}$ (Fig. 11 (a, b)).

There are two possibilities for the arrangement of the point of this instability $(\rho_{\text{cr}}^{(\text{FJ})}, q_{\text{cr}}^{(\text{FJ})})$ on the fundamental diagram in the OV model and other models in the context of the fundamental diagram approach:

(i) The point $(\rho_{\text{cr}}^{(\text{FJ})}, q_{\text{cr}}^{(\text{FJ})})$ lies left of the maximum point of the fundamental diagram (ρ_0, q_0) , i.e., on the branch of the diagram with a positive slope (Fig. 11 (a)):

$$\rho = \rho_{\text{cr}}^{(\text{FJ})} < \rho_0 \quad (53)$$

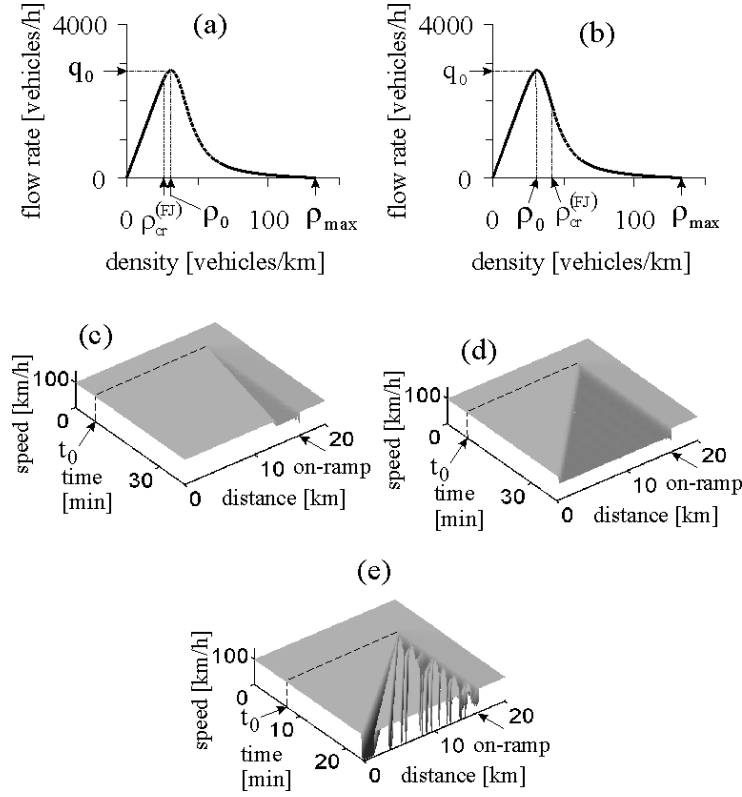


Figure 11. Traffic patterns in OV-models at an on-ramp bottleneck: (a, b) – Fundamental diagrams of OV-models when the condition (53) (a) and (54) (b) are satisfied, respectively. (c, d) – Widening patterns of dense flow upstream of the bottleneck at two flow rates $q_{on} = 160$ (c) and 400 (d) vehicles/h. (e) – Formation of wide moving jams within the dense flow upstream of the bottleneck at $q_{on} = 700$ vehicles/h. In (c–e) the flow rate $q_{in} = 2676$ vehicles/h. Figures (c–e) are related to the OV-model (b) at $V(g) = V_0 \left(\tanh((g - g_0)/g_1) + \tanh(g_0/g_1) \right)$ at $V_0 = 14$ m/s, $g_0 = 17$ m, $g_1 = 7$ m, the sensitivity $A(g, v) = A(v)$ in (49) is $A(v) = 5$ at $v \geq 12$ m/s and $A(v) = 0.9$ at $v < 12$ m/s.

(ii) The point $(\rho_{\text{cr}}^{(\text{FJ})}, q_{\text{cr}}^{(\text{FJ})})$ lies right of the maximum point of the fundamental diagram (ρ_0, q_0) , i.e., on the branch of the diagram with a negative slope (Fig. 11 (b)):

$$\rho = \rho_{\text{cr}}^{(\text{FJ})} > \rho_0. \quad (54)$$

Note that in both cases (i) and (ii) all states on the fundamental diagram, in which the density satisfies the condition

$$\rho_{\text{min}} \leq \rho < \rho_{\text{cr}}^{(\text{FJ})}, \quad (55)$$

where ρ_{min} is the density in the wide moving jam outflow associated with the flow rate q_{out} , are metastable states with respect to an F→J transition.

The case (i) has intensively been considered in the literature [3, 4, 5, 6]. On a homogeneous road as well as at an on-ramp bottleneck an F→J transition occurs spontaneously, when the flow rate q_{in} is large enough [42, 25, 22, 26, 27, 4]. Thus, the onset of congestion in these models is associated with the F→J transition. As mentioned in Sect. 1, this model result is inconsistent with empirical observations in which a first-order F→S transition governs the onset of congestion in free flow.

In the case (ii) (Fig. 11 (b)), the flow rate in free flow downstream of an on-ramp bottleneck q_{sum} cannot exceed the maximum flow rate on the fundamental diagram q_0 . If q_{in} is a given large enough value and the flow rate q_{on} begins to increase, then a localized perturbation that has qualitatively the same features as in the ATD- and SA-models (Sect. 4.2) appears in a neighborhood of the bottleneck (Fig. 12 (a, b)). In particular, the minimum speed $v_{\text{free}}^{(\text{B})}$ within the perturbation decreases when q_{on} increases (points 1–4 in Fig. 12 (c)). In the OV-model, when q_{on} increases, the location of the minimum speed $v_{\text{free}}^{(\text{B})}$ within the perturbation exhibits firstly a slight shift downstream and then upstream within the merging region of the on-ramp (Fig. 12 (a, b)). For this reason, the flow rate on the main road at the location of the minimum speed $v_{\text{free}}^{(\text{B})}$ firstly slightly increases and then decreases (points 1–4 in Fig. 12 (e)), whereas the flow rate on the main road upstream of the on-ramp merging region is equal to q_{in} (points 1–4 in Fig. 12 (d)).

At a given large enough flow rate q_{in} this growth of the local perturbation with q_{on} has a limit. This limit is reached when the flow rate q_{sum} approaches the maximum flow rate on the fundamental diagram:

$$q_{\text{sum}}^{(\text{max})} = q_{\text{in}} + q_{\text{on}} = q_0. \quad (56)$$

When the flow rate q_{on} further increases, i.e.,

$$\Delta q = q_{\text{in}} + q_{\text{on}} - q_0 > 0, \quad (57)$$

then upstream of the bottleneck a dense traffic flow with the density $\rho_{\text{d}} > \rho_0$ and flow rate $q_{\text{d}} < q_0$ associated with the branch of the diagram with a negative slope occurs (Fig. 11 (c, d)). The greater the flow rate q_{on} , specifically the greater Δq (57), the greater the velocity of the upstream front of this dense flow (Fig. 11 (c, d)) and the lower vehicle speed within the dense flow (points 5, 6 in Fig. 12 (c)).

This widening dense flow upstream of the bottleneck can exist only, when the density ρ_{d} in the dense flow satisfies the condition

$$\rho_0 < \rho_{\text{d}} < \rho_{\text{cr}}^{(\text{FJ})}. \quad (58)$$

This is because at the density $\rho_{\text{d}} = \rho_{\text{cr}}^{(\text{FJ})}$ the dense flow loses its stability against wide moving jam emergence (point 7 and dotted down-arrow in Fig. 12 (c)). Due to

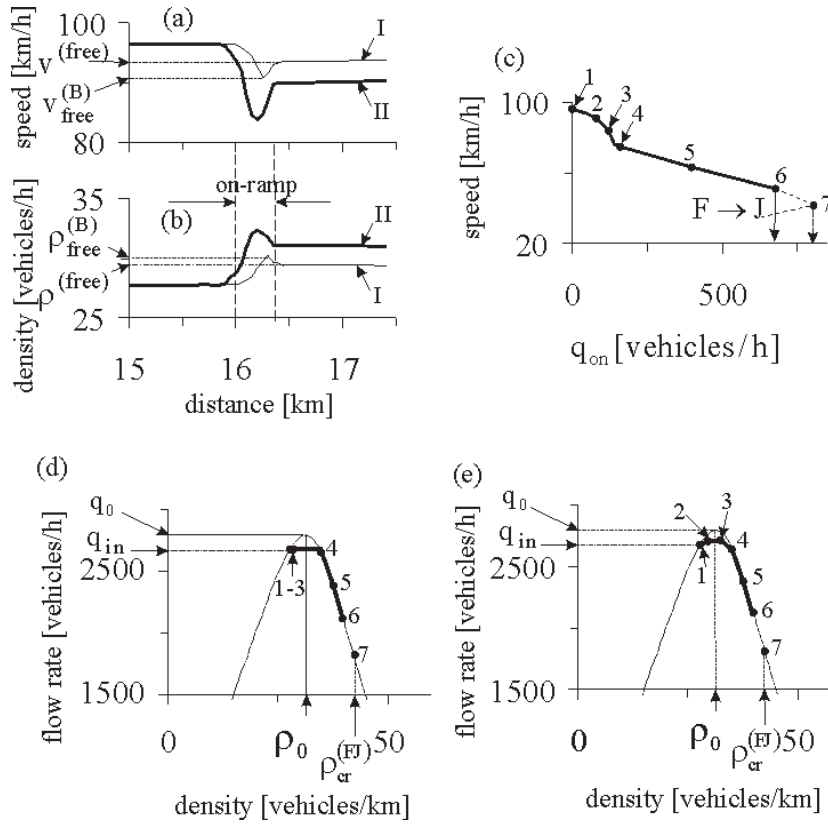


Figure 12. Pattern evolution in the OV-model in Fig. 11 (b) at an on-ramp bottleneck: (a, b) – averaged speed (5-min averaged data) (a) and density (b) as freeway location functions within the deterministic perturbation localized at the bottleneck at different flow rates. $q_{on} = 80$ (curve I) and 120 (curve II) vehicles/h. (c, d) – On-ramp flow rate dependences of the speed (c), flow rate and density (d, e) within patterns at the bottleneck. Dotted curves on Fig. (d, e) show steady model states in the flow–density plane. $q_{in} = 2676$ vehicles/h.

large fluctuations at the bottleneck, in numerical simulations this instability occurs already at the density $\rho_d < \rho_{cr}^{(FJ)}$. This confirms that wide moving jam emergence is associated with a first-order phase transition (point 6 and solid down-arrow in Fig. 12 (c)).

The congested patterns in Fig. 11 (c, d) at the first glance resemble a widening SP and an GP, respectively. Indeed, in both cases a dense flow occurs upstream of the bottleneck whose downstream front is fixed at the bottleneck. Thus, this dense flow should satisfy the macroscopic spatiotemporal objective criteria for the synchronized flow phase (Sect. 1). This conclusion is, however, incorrect. To explain this, note that in *empirical* observations application of the objective criteria for the traffic phases in congested traffic leads to clear distinction of the synchronized flow phase. This is because in this case this *empirical* traffic flow exhibits all necessary features of synchronized flow. One of the most important features is the probabilistic nature of synchronized flow emergence in free flow, i.e., that an F→S transition is a first-order phase transition. In contrast, in a traffic flow *theory* application of the objective criteria does not guarantee that a dense traffic flow exhibits the probabilistic nature of synchronized flow emergence.

This conclusion concerns the OV model under the condition (54) (Fig. 11 (b)) as well as in other models in the context of the fundamental diagram approach. Whereas for the SA-model there is a Z-shaped speed–flow rate characteristic associated with the probabilistic nature of synchronized flow emergence in free flow at the bottleneck (Fig. 4 (c–e)), for the OV-model the on-ramp flow rate dependence of the speed at the bottleneck is a *monotonous* decreasing function (Fig. 12 (c)): There is no first-order phase transition, when a dense flow related to the fundamental diagram with a negative slope is formed upstream of the bottleneck. Thus, the dense traffic flow in the case OV-model and other models in the context of the fundamental diagram approach does not exhibit the important empirical feature of synchronized flow and, therefore, the dense flow is not associated with the synchronized flow phase.

This dense flow occurs due to maximum point on the fundamental diagram (point (ρ_0, q_0) in (Fig. 11 (b)) and a spatial non-homogeneity on the road caused by the bottleneck. In other words, rather than a probabilistic nucleation effect that is shown by empirical synchronized flow, this dense flow occurs on a deterministic way. There is no hysteresis and there is no speed drop that are characteristic for empirical synchronized flow emergence at the bottleneck, when dense flow is formed upstream of the bottleneck after the flow rate q_{sum} exceeds q_0 associated with the maximum point (ρ_0, q_0) on the fundamental diagram (Fig. 12 (c)). Thus, this dense flow together with free flow associated with the branch of the fundamental diagram with a positive slope can be considered the free flow phase. Only when the density in this dense flow approaches the critical density $\rho_{cr}^{(FJ)}$ moving jams begin to emerge in this dense flow. Consequently, the point $(\rho_{cr}^{(FJ)}, q_{cr}^{(FJ)})$ on the fundamental diagram can be considered as the critical point for an F→J transition in the OV-model.

We see that all effects of different pattern formation at the bottleneck in the OV-models as well as in other models in the context of the fundamental diagram approach are model effects only, which have no relation to empirical observations of congested traffic patterns [7]. The only one exception is characteristic parameters of wide moving jam propagation first discovered in [42].

5.3. Conclusions

(i) Two different deterministic microscopic traffic flow model classes in the context of three-phase traffic theory, the ATD- and SA-models, have been introduced in the article.

(ii) The ATD- and SA-models reproduce most important *empirical* spatiotemporal features of phase transitions in traffic flow and congested traffic patterns.

(iii) In contrast with all other known deterministic microscopic traffic flow models, in the ATD- and SA-models vehicles moving in free flow and vehicles moving in synchronized flow exhibit qualitatively different dynamic behavior. This is a result of the introduction of two separated regions of steady state model solutions for free flow and synchronized flow in the ATD- and SA-models as well as different dynamic rules of vehicle motion in free flow and synchronized flow implemented in the models.

(iv) There is a first-order phase transition in the ATD- and SA-models from free flow to synchronized flow. This means that the ATD- and SA-models exhibit the probabilistic nature of an $F \rightarrow S$ transition at the bottleneck observed in empirical observations.

(v) The probabilistic nature of the onset of congestion in free flow at the bottleneck that the ATD- and SA-models show is also associated with metastability of free flow at the bottleneck against external short-time disturbances in this flow in a neighborhood of the bottleneck. As a result, there is multiple congested pattern emergence in an initial free flow at the bottleneck in the ATD- and SA-models: Depending on an amplitude (or duration) of an external disturbance, one of the SPs or else an GP can be induced in free flow at the bottleneck at the same chosen model parameters.

(v) In accordance with empirical results, in the ATD- and SA-models moving jams can emerge spontaneously in synchronized flow only, i.e., as a result of $F \rightarrow S \rightarrow J$ transitions.

(vi) In addition to the above common behavior of the ATD- and SA-models, these models exhibit also some qualitatively different features. This is because in the ATD-model synchronized flow model steady states are related to a 2D-region in the flow–density plane, whereas synchronized flow model steady states in the SA-models belong to an 1D-region (a curve) in the flow–density plane. In particular, the following differences of model features have been found:

(1) The ATD-model can show all types of spatiotemporal congested patterns at an on-ramp bottleneck observed in empirical observations. The ADT-model exhibits qualitatively the same diagram of congested patterns at the bottleneck as those in microscopic stochastic models in the context of three-phase traffic theory of Ref. [33].

(2) In contrast, whereas WSPs and GPs can also be reproduced by SA-models, these models cannot show LSPs associated with empirical results as well as different states of synchronized flow in the wide moving jam outflows.

(vii) Deterministic models in the context of the fundamental diagram approach (see references in [4]) cannot explain the onset of congestion in free flow, which in empirical observations are associated with a first-order $F \rightarrow S$ transition. In these models, when the density in free flow at the bottleneck exceeds the density associated with the maximum point at the fundamental diagram, widening dense traffic flow occurs upstream of an on-ramp bottleneck. In contrast with empirical observations, there is no nucleation of this dense traffic flow in an initial free flow at the bottleneck: This model dense flow results from non-homogeneity of a freeway in a neighborhood of the bottleneck. Thus, these models cannot show the probabilistic nature of

the onset of congestion at the bottleneck. However, the probabilistic nature is the fundamental empirical feature of the onset of congestion in free flow with the subsequent synchronized flow phase emergence at the bottleneck. In other words, this dense traffic flow is not to be identified as synchronized flow, i.e., this dense flow is a model effect only, which has no relation to real traffic flow.

Appendix A.

To derive the formula (12) for the safety acceleration, let us use the concept of safety speed v_s proposed by Gipps [41]. A simple condition for the safety speed v_s can be written as follows:

$$v_s T_s + v_s^2 / (2b_s) \leq g + v_\ell^2 / (2b_s), \quad (\text{A.1})$$

where b_s is a constant deceleration. When (A.1) is an equality, the formula (A.1) gives the equation for the speed v_s as a function of space gap g and the preceding vehicle speed v_ℓ . The solution of this equation can be written as:

$$v_s(g, v_\ell) = \frac{2b_s g + v_\ell^2}{b_s T_s + \sqrt{b_s^2 T_s^2 + 2b_s g + v_\ell^2}}. \quad (\text{A.2})$$

From (A.1), (A.2) it can be seen that if $g = v_\ell T_s$, the safety speed v_s equals v_ℓ . Since the vehicle speed v cannot exceed the safe speed, and hence $v \leq v_s = v_\ell$ at $g = v_\ell T_s$, the space gap g cannot become smaller than $v_\ell T_s$. In particular, this ensures the collision-free vehicle motion in models with safety speed. The condition $g \geq v_\ell T_s$ can be used, to simplify the formula (A.2). For this purpose, the space gap g in denominator of (A.2) can be replaced by the value $v_\ell T_s$. Then formula (A.2) reads

$$v_s(g, v_\ell) = \frac{g + v_\ell^2 / (2b_s)}{T_s + v_\ell / (2b_s)}. \quad (\text{A.3})$$

Let us define the safety acceleration a_s as an acceleration needed for the driver to reach the safety speed v_s at time $t_1 = t + T_0$, provided the vehicle moves with the speed v at time t :

$$a_s = \frac{v_s(g(t_1), v_\ell(t_1)) - v(t)}{T_0}, \quad (\text{A.4})$$

where T_0 is a constant equal or greater than the minimum driver time delay. Neglecting the changes in vehicle speeds v and v_ℓ during the time T_0 , and estimating the space gap g at time t_1 as $g(t_1) = g(t) + (v_\ell(t) - v(t))T_0$, from (A.3), (A.4) we get:

$$a_s(g, v, v_\ell) = \frac{g - v T_s + (T_0 + v_\ell / (2b_s))(v_\ell - v)}{T_0(T_s + v_\ell / (2b_s))}, \quad (\text{A.5})$$

where all values are related to the same time moment t .

In the microscopic model this formula for the safety acceleration a_s (12) is used with a heuristic coefficient α and at $b = 2b_s$.

Appendix B.

In this Appendix, two further variants of the SA-models are presented. In the first of these variants, the formula (28) reads as follows

$$\frac{dv}{dt} = \begin{cases} a^{(\text{free})} & \text{at } g \geq g_{\min}^{(\text{free})}, \\ a^{(\text{syn})} & \text{at } g_{\max}^{(\text{jam})} < g < g_{\min}^{(\text{free})}, \\ a^{(\text{jam})} & \text{at } 0 \leq g \leq g_{\max}^{(\text{jam})}, \end{cases} \quad (\text{B.1})$$

where $a^{(\text{free})}$, $a^{(\text{syn})}$, $a^{(\text{jam})}$ are given by (29)–(33). In this SA-model, steady states of free flow (the curve F in Fig. 2 (e)) correspond to the condition (35), averaged steady states of synchronized flow are related to a line S given by the condition

$$q = (1 - \rho/\rho_{\min}^{(\text{jam})})/T_{\text{av}}^{(\text{syn})} \quad \text{at } \rho_{\max}^{(\text{free})} < \rho < \rho_{\min}^{(\text{jam})}, \quad (\text{B.2})$$

steady states for a wide moving jam are associated with the condition (39) (Fig. 2 (e)).

In the second SA-model, formula (28) reads as follows

$$\frac{dv}{dt} = \begin{cases} a^{(\text{free})} & \text{at } g \geq g_{\min}^{(\text{free})}, \\ a^{(\text{FS})} & \text{at } g_{\max}^{(\text{syn})} < g < g_{\min}^{(\text{free})}, \\ a^{(\text{syn})} & \text{at } g_{\max}^{(\text{jam})} < g < g_{\max}^{(\text{syn})}, \\ a^{(\text{jam})} & \text{at } 0 \leq g \leq g_{\max}^{(\text{jam})}, \end{cases} \quad (\text{B.3})$$

where $a^{(\text{free})}$, $a^{(\text{syn})}$, $a^{(\text{jam})}$ are given by (29)–(33); $g_{\max}^{(\text{syn})}$ is the maximum space gap in the synchronized flow. A function $a^{(\text{FS})}(g, v, v_\ell)$ in (B.3) is taken as follows

$$a^{(\text{FS})}(g, v, v_\ell) = \min(A^{(\text{FS})}(V^{(\text{FS})}(g) - v) + K^{(\text{FS})}(v, v_\ell)(v_\ell - v), a_{\max}), \quad (\text{B.4})$$

where $A^{(\text{FS})} = A^{(\text{syn})}$, $K^{(\text{FS})} = K^{(\text{syn})}$; $V^{(\text{FS})}(g)$ is chosen as a linear function between points $(g_{\min}^{(\text{free})}, v_{\min}^{(\text{free})})$ and $(g_{\max}^{(\text{syn})}, v_{\max}^{(\text{syn})})$:

$$V^{(\text{FS})}(g) = v_{\min}^{(\text{free})} + (v_{\max}^{(\text{syn})} - v_{\min}^{(\text{free})}) \frac{g_{\min}^{(\text{free})} - g}{g_{\min}^{(\text{free})} - g_{\max}^{(\text{syn})}}, \quad (\text{B.5})$$

where $v_{\max}^{(\text{syn})} = (g_{\max}^{(\text{syn})} - g_{\max}^{(\text{jam})})/T_{\text{av}}^{(\text{syn})}$.

In the SA-model (B.3), steady states of free flow (the curve F in Fig. 2 (f)) are associated with the condition (35), averaged steady states of synchronized flow are related to a line S given by the condition

$$q = (1 - \rho/\rho_{\min}^{(\text{jam})})/T_{\text{av}}^{(\text{syn})} \quad \text{at } \rho_{\min}^{(\text{syn})} < \rho < \rho_{\min}^{(\text{jam})}, \quad (\text{B.6})$$

where $\rho_{\min}^{(\text{syn})} = 1/(g_{\max}^{(\text{syn})} + d)$, and steady states for a wide moving jam are found from the condition (39) (Fig. 2 (f)).

In contrast with the other SA-models, the SA-model (B.3) has a limited density range of steady states between steady states for free flow and synchronized flow, which are found from the condition

$$a^{(\text{FS})} = 0 \quad \text{at } g_{\max}^{(\text{syn})} < g < g_{\min}^{(\text{free})}. \quad (\text{B.7})$$

This condition yields the equation for the line FS with a negative slope in the flow-density plane (Fig. 2 (d))

$$q = q_{\max}^{(\text{free})} + (q_{\max}^{(\text{syn})} - q_{\max}^{(\text{free})}) \frac{\rho_{\max}^{(\text{free})} - \rho}{\rho_{\max}^{(\text{free})} - \rho_{\min}^{(\text{syn})}} \quad \text{at } \rho_{\max}^{(\text{free})} < \rho < \rho_{\min}^{(\text{syn})}, \quad (\text{B.8})$$

where $q_{\max}^{(\text{syn})} = \rho_{\min}^{(\text{syn})} v_{\max}^{(\text{syn})}$. The steady state model solutions (B.8) should be unstable against infinitesimal non-homogeneous perturbations that can be satisfied through an appropriated choice of the value $q_{\max}^{(\text{syn})}$. These solutions are used to simulate $F \rightarrow S$ and $S \rightarrow F$ transitions in the SA-model (B.3).

- [1] N.H. Gartner, C.J. Messer, A. Rathi (eds.). *Special Report 165: Revised Monograph on Traffic Flow Theory* (Transportation Research Board, Washington, D.C. 1997)
- [2] D.E. Wolf. *Physica A* **263**, 438 (1999)
- [3] D. Chowdhury, L. Santen, A. Schadschneider. *Physics Reports* **329**, 199 (2000)
- [4] D. Helbing. *Rev. Mod. Phys.* **73**, 1067–1141 (2001)
- [5] T. Nagatani. *Rep. Prog. Phys.* **65**, 1331–1386 (2002)
- [6] K. Nagel, P. Wagner, R. Woessler. *Operation Res.* **51**, 681–716 (2003)
- [7] B.S. Kerner. *The Physics of Traffic* (Springer, Berlin, New York 2004).
- [8] J.-B. Lesort (editor). *Transportation and Traffic Theory*, Proceedings of the 13th International Symposium on Transportation and Traffic Theory (Elsevier Science Ltd, Oxford 1996)
- [9] A. Ceder (editor). *Transportation and Traffic Theory*, Proceedings of the 14th International Symposium on Transportation and Traffic Theory (Elsevier Science Ltd, Oxford 1999)
- [10] M.A.P. Taylor (editor). *Transportation and Traffic Theory in the 21st Century*, Proceedings of the 15th International Symposium on Transportation and Traffic Theory (Elsevier Science Ltd, Amsterdam 2002)
- [11] D.E. Wolf, M. Schreckenberg, A. Bachem (editors). *Traffic and Granular Flow*, Proceedings of the International Workshop on Traffic and Granular Flow, October 1995 (World Scientific, Singapore 1995)
- [12] M. Schreckenberg, D.E. Wolf (editors). *Traffic and Granular Flow' 97*, Proceedings of the International Workshop on Traffic and Granular Flow, October 1997 (Springer, Singapore 1998)
- [13] D. Helbing, H.J. Herrmann, M. Schreckenberg, D.E. Wolf (editors). *Traffic and Granular Flow' 99*, Proceedings of the International Workshop on Traffic and Granular Flow, October 1999, (Springer, Heidelberg 2000)
- [14] M. Fukui, Y. Sugiyama, M. Schreckenberg, D.E. Wolf (editors). *Traffic and Granular Flow' 01*, Proceedings of the International Workshop on Traffic and Granular Flow, October 2001, (Springer, Heidelberg 2003)
- [15] S.P. Hoogendoorn, P.H.L. Bovy, M. Schreckenberg, D.E. Wolf (editors). *Traffic and Granular Flow' 03*, Proceedings of the International Workshop on Traffic and Granular Flow, October 2003, (Springer, Heidelberg 2004) (in press)
- [16] R. Herman, E.W. Montroll, R.B. Potts, R.W. Rothery. *Operations Res.* **7**, 86–106 (1959).
- [17] D. C. Gazis, R. Herman, and R. W. Rothery, *Operations Res.* **9**, 545–567 (1961).
- [18] T. Nagatani and K. Nakanishi, *Phys. Rev. E* **57**, 6415 (1998).
- [19] I. Lubashevsky, P. Wagner, R. Mahnke, *European Phys. J. B* **32**, 243–247 (2003).
- [20] G.F. Newell, *Operations Res.* **9**, 209 (1961).
- [21] G.B. Whitham, *Proc. R. Soc. London A* **428**, 49 (1990).
- [22] M. Bando, K. Hasebe, A. Nakayama, A. Shibata, Y. Sugiyama, *Jpn. J. Appl. Math.* **11**, 203 (1994); *Phys. Rev. E* **51**, 1035–1042 (1995).
- [23] M. Treiber, D. Helbing, e-print, cond-mat/9901239 (1999).
- [24] M. Treiber, A. Hennecke, D. Helbing, *Phys. Rev. E* **62**, 1805–1824 (2000).
- [25] B.S. Kerner, P. Konhäuser, M. Schilke, *Phys. Rev. E* **51**, 6243–6246 (1995).
- [26] D. Helbing, A. Hennecke, M. Treiber: *Phys. Rev. Lett.* **82**, 4360 (1999)
- [27] H.Y. Lee, H.-W. Lee, D. Kim: *Phys. Rev. E* **59**, 5101 (1999)
- [28] B. S. Kerner, *Phys. Rev. Lett.* **81**, 3797 (1998).
- [29] B. S. Kerner, *Phys. Rev. E* **65**, 046138 (2002).
- [30] L. Elefteriadou, R.P. Roess, W.R. McShane, *Transportation Research Record* **1484**, 80–89 (1995).
- [31] B.N. Persaud, S. Yagar, R. Brownlee: *Transportation Research Record* **1634**, 64–69 (1998).
- [32] M. Lorenz, L. Elefteriadou, *Transportation Research Circular* **E-C018**, 84–95 (2000).
- [33] B.S. Kerner, S.L. Klenov: *J. Phys. A: Math. Gen.* **35**, L31 (2002)
- [34] B.S. Kerner, S.L. Klenov, D.E. Wolf, *J. Phys. A: Math. Gen.* **35** 9971–10013 (2002).
- [35] B.S. Kerner, S.L. Klenov, *Phys. Rev.* **68** 036130 (2003)
- [36] B.S. Kerner, S.L. Klenov, *J. Phys. A: Math. Gen.* **37** 8753–8788 (2004).
- [37] B.S. Kerner, S.L. Klenov, H. Hiller. physics/0507094 (2005). E-print in <http://arxiv.org/abs/physics/0507094>.
- [38] L.C. Davis, *Phys. Rev. E* **69** 016108 (2004).
- [39] H.K. Lee, R. Barlović, M. Schreckenberg, D. Kim, *Phys. Rev. Lett.* **92**, 238702 (2004).
- [40] R. Jiang, Q.S. Wu, *J. Phys. A: Math. Gen.* **37**, 8197–8213 (2004).
- [41] P.G. Gipps, *Trans. Res. B.* **15**, 105–111 (1981).
- [42] B.S. Kerner, P. Konhäuser. *Phys. Rev. E* **50**, 54–83 (1994).